

AD/A-002 709

ENERGY ABSORPTION AND IMPACT BEHAVIOR  
OF STIFFENED AND UNSTIFFENED ALUMINUM  
PANELS

A. J. Furio, Jr., et al

Naval Ship Research and Development Center  
Bethesda, Maryland

November 1974

DISTRIBUTED BY:

**NTIS**

National Technical Information Service  
U. S. DEPARTMENT OF COMMERCE

UNCLASSIFIED

AD/A002709

SECURITY CLASSIFICATION OF THIS PAGE (When Data Entered)

REPORT DOCUMENTATION PAGE		READ INSTRUCTIONS BEFORE COMPLETING FORM
1. REPORT NUMBER 4499	2. GOVT ACCESSION NO.	3. RECIPIENT'S CATALOG NUMBER
4. TITLE (and Subtitle) ENERGY ABSORPTION AND IMPACT BEHAVIOR OF STIFFENED AND UNSTIFFENED ALUMINUM PANELS		5. TYPE OF REPORT & PERIOD COVERED
		6. PERFORMING ORG. REPORT NUMBER
7. AUTHOR(s) A.J. Furio, Jr. and W.E. Gilbert		8. CONTRACT OR GRANT NUMBER(s)
9. PERFORMING ORGANIZATION NAME AND ADDRESS Naval Ship Research and Development Center Bethesda, Maryland 20084		10. PROGRAM ELEMENT, PROJECT, TASK AREA & WORK UNIT NUMBERS ARPA Order 1676, Program Code ON10 Task Area SF 43.422.703-12 Task 17934 Work Unit 1-1130-600
11. CONTROLLING OFFICE NAME AND ADDRESS Advanced Research Projects Agency		12. REPORT DATE November 1974
		13. NUMBER OF PAGES 74 10
14. MONITORING AGENCY NAME & ADDRESS (if different from Controlling Office)		15. SECURITY CLASS. (of this report) UNCLASSIFIED
		15a. DECLASSIFICATION/DOWNGRADING SCHEDULE
16. DISTRIBUTION STATEMENT (of this Report) APPROVED FOR PUBLIC RELEASE: DISTRIBUTION UNLIMITED		
17. DISTRIBUTION STATEMENT (of the abstract entered in Block 20, if different from Report)		
18. SUPPLEMENTARY NOTES Reproduced by NATIONAL TECHNICAL INFORMATION SERVICE US Department of Commerce Springfield, VA. 22151		
19. KEY WORDS (Continue on reverse side if necessary and identify by block number) Arctic Surface Effect Vehicles      Underbody Protection      Closed-cell foam Impact      Panels      Bending-type behavior Collision      Web stiffened      Membrane-type behavior Flanged stiffeners      (Item 19 continued on back)		
20. ABSTRACT (Continue on reverse side if necessary and identify by block number) The impact behavior of stiffened and unstiffened square aluminum panels under fixed boundary conditions was investigated experimentally and theoretically, and the ultimate energy-absorbing characteristics were determined as a function of geometry. The effect of rigid, closed-cell foam (2-lb/ft <sup>3</sup> urethane) on an unstiffened panel was also investigated. (Continued on reverse side)		

DD FORM 1 JAN 73 1473

EDITION OF 1 NOV 68 IS OBSOLETE  
S/N 0102-014-6601

UNCLASSIFIED

SECURITY CLASSIFICATION OF THIS PAGE (When Data Entered)

**UNCLASSIFIED**

**SECURITY CLASSIFICATION OF THIS PAGE(When Data Entered)**

(Block 19 continued)

Comparison of Experimental Results  
and Theoretical Predictions

(Block 20 continued)

A geometric scaling law was developed to extrapolate experimental results to sizes needed for the underbody collision protection system of surface effect vehicles for Arctic operation. Protection levels were determined as a function of allowable vertical impact velocity and craft weight.

11

**UNCLASSIFIED**

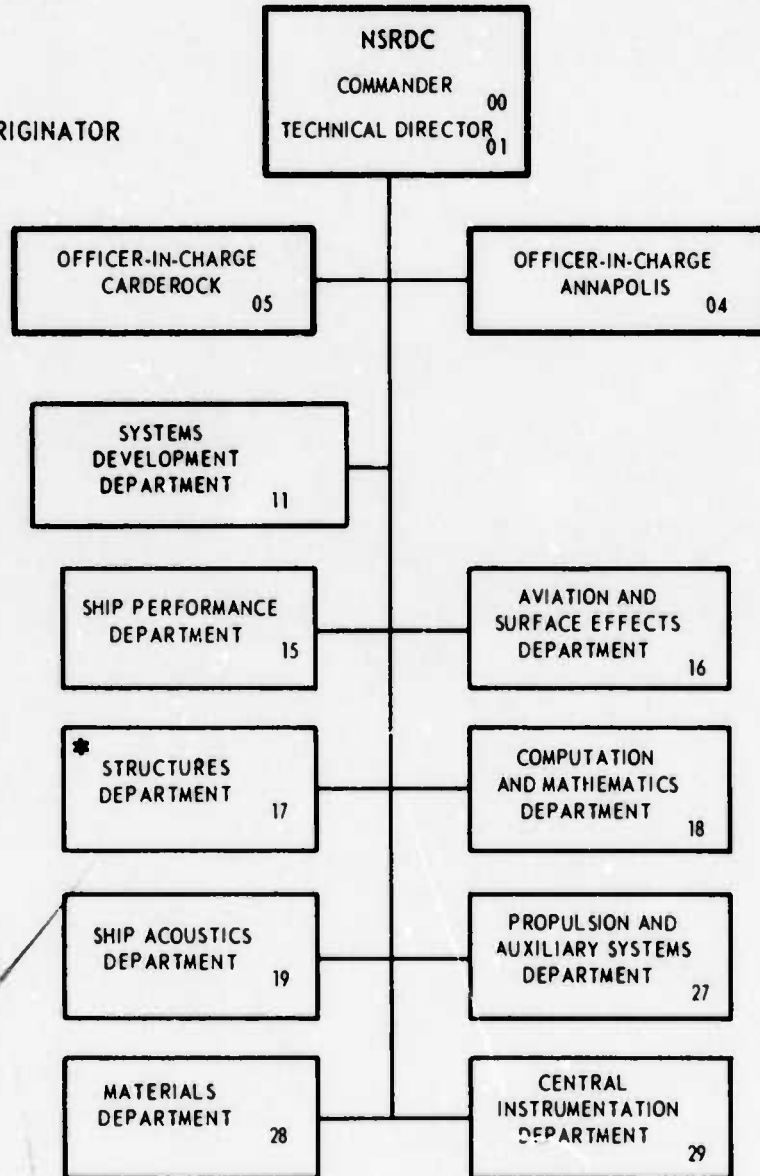
**SECURITY CLASSIFICATION OF THIS PAGE(When Data Entered)**

The Naval Ship Research and Development Center is a U. S. Navy center for laboratory effort directed at achieving improved sea and air vehicles. It was formed in March 1967 by merging the David Taylor Model Basin at Carderock, Maryland with the Marine Engineering Laboratory at Annapolis, Maryland.

Naval Ship Research and Development Center  
Bethesda, Md. 20084

### MAJOR NSRDC ORGANIZATIONAL COMPONENTS

\*REPORT ORIGINATOR



APPROVAL

BY: [Signature]

DATE: [Blank]

1A

## TABLE OF CONTENTS

	Page
ABSTRACT . . . . .	I
ADMINISTRATIVE INFORMATION . . . . .	I
INTRODUCTION . . . . .	I
EXPERIMENTAL DETERMINATION OF PANEL RESPONSE . . . . .	3
EXPERIMENTAL SETUP . . . . .	3
INSTRUMENTATION . . . . .	5
PANEL GEOMETRY AND FABRICATION . . . . .	6
TEST RESULTS . . . . .	6
RESPONSE CHARACTERIZATION . . . . .	6
DATA REDUCTION PROCESS . . . . .	9
ENERGY ABSORPTION . . . . .	12
Effect of Panel Geometry . . . . .	16
Effect of Repeated Loading . . . . .	21
Effect of Energy-Absorbing Foam . . . . .	21
THEORETICAL DETERMINATION OF THE LOAD- DEFLECTION CURVES . . . . .	26
UNSTIFFENED SQUARE PLATES . . . . .	26
STIFFENED SQUARE PLATES . . . . .	31
LOAD-DEFLECTION RELATIONSHIP FOR STIFFENED PANELS . . . . .	32
COMPARISON OF THEORETICAL AND EXPERIMENTAL RESULTS . . . . .	35
APPLICATIONS OF THE ENERGY-ABSORBING UNDERBODY PANEL FOR ASEV'S . . . . .	45
CONCLUSIONS . . . . .	51
ACKNOWLEDGMENT . . . . .	53
APPENDIX A – DERIVATION OF PROTRUSION DEFLECTION DEFINITION . . . . .	55
APPENDIX B – DERIVATION OF MEMBRANE STRESS . . . . .	57

	Page
APPENDIX C – FREE-BODY DIAGRAM AND DERIVATION OF THE LOAD-DEFLECTION EQUATION . . . . .	59
APPENDIX D – DIMENSIONAL ANALYSIS OF ENERGY SCALING LAWS . . . . .	61

### LIST OF FIGURES

1 – 10-Ton ASEV (SK-5) Test Craft Navigating an Ice Obstacle . . . . .	2
2 – “Ski Jumping” an Ice Obstacle . . . . .	2
3 – NSRDC Drop Test Tower Facility . . . . .	4
4 – Panel Testing Fixture . . . . .	5
5 – Characteristic Acceleration-Time Traces for Various Panel Geometries . . . . .	7
6 – Acceleration-Time History of Unstiffened Panel . . . . .	8
7 – Acceleration-Time History of Web-Stiffened Panel . . . . .	10
8 – Acceleration-Time History of Panel with Flanged Stiffeners . . . . .	11
9 – Closeup of Welding Failure in the Heat-Affected Zone . . . . .	12
10 – Test Data Used for Computer Program . . . . .	13
11 – Typical Computer Printout of Panel Response . . . . .	15
12 – Panel Response as a Function of Energy Absorption . . . . .	17
13 – (2 x 2) Panel with Flanged Stiffeners after Impact . . . . .	18
14 – (3 x 0) Panel with Flanged Stiffeners before Impact . . . . .	19
15 – Specific Energy Absorption for Selected Test Series . . . . .	20
16 – Damage Sustained by a (3 x 0) Panel with Flanged Stiffeners during Successive Impacts . . . . .	22
17 – Load-Deflection Curves for Successive Impacts on a (3 x 0) Panel with Flanged Stiffeners . . . . .	23
18 – Response of an Unstiffened Panel with Energy-Absorbing Foam . . . . .	24
19 – Comparison of Load-Deflection Curves for a Panel with and without Energy-Absorbing Foam . . . . .	25

	Page
20 – Statically Loaded Circular Panel with Fixed Boundary . . . . .	26
21 – Local Protrusion and Radius of Loading Area for Unstiffened Panel . . . . .	29
22 – Theoretical versus Experimental Load-Deflection Curves for Aluminum Unstiffened Panels . . . . .	30
23 – Effective Width of a (1 X 1) Web-Stiffened Panel . . . . .	31
24 – Stress Profile Assuming Combined Bending and Membrane Response . . . . .	33
25 – Theoretical versus Experimental Load-Deflection Curves for Aluminum Web-Stiffened Panel–Type I . . . . .	36
26 – Theoretical versus Experimental Load-Deflection Curves for Aluminum Web-Stiffened Panel–Type II . . . . .	37
27 – Theoretical versus Experimental Load-Deflection Curves for Aluminum Web-Stiffened Panel–Type III . . . . .	38
28 – Theoretical versus Experimental Load-Deflection Curves for Aluminum Web-Stiffened Panel–Type IV . . . . .	39
29 – Theoretical versus Experimental Load-Deflection Curves for Aluminum Web-Stiffened Panel–Type V . . . . .	40
30 – Theoretical versus Experimental Load-Deflection Curves for Aluminum Web-Stiffened Panel–Type VI . . . . .	41
31 – Theoretical versus Experimental Load-Deflection Curves for Aluminum Web-Stiffened Panel–Type VII . . . . .	42
32 – Theoretical versus Experimental Load-Deflection Curves for Aluminum Web-Stiffened Panel–Type VIII . . . . .	43
33 – Underbody of SK-5 following Impact on an Ice Obstacle during 1971 SEV Arctic Trials . . . . .	45
34 – Vertical Kinetic Energy of 150- and 540-Ton ASEV's as a Function of Impact Velocity . . . . .	47
35 – Energy-Absorbing Capacity versus Scale Factor . . . . .	49
36 – Weight of Collision Protection System as a Function of Maximum Impact Velocity . . . . .	50
37 – Weight of Collision Protection System as a Function of Allowable Impact Velocity . . . . .	52

	Page
20 - Statically Loaded Circular Panel with Fixed Boundary . . . . .	26
21 - Local Protrusion and Radius of Loading Area for Unstiffened Panel . . . . .	29
22 - Theoretical versus Experimental Load-Deflection Curves for Aluminum Unstiffened Panels . . . . .	30
23 - Effective Width of a (1 X 1) Web-Stiffened Panel . . . . .	31
24 - Stress Profile Assuming Combined Bending and Membrane Response . . . . .	33
25 - Theoretical versus Experimental Load-Deflection Curves for Aluminum Web-Stiffened Panel-Type I . . . . .	36
26 - Theoretical versus Experimental Load-Deflection Curves for Aluminum Web-Stiffened Panel-Type II . . . . .	37
27 - Theoretical versus Experimental Load-Deflection Curves for Aluminum Web-Stiffened Panel-Type III . . . . .	38
28 - Theoretical versus Experimental Load-Deflection Curves for Aluminum Web-Stiffened Panel-Type IV . . . . .	39
29 - Theoretical versus Experimental Load-Deflection Curves for Aluminum Web-Stiffened Panel-Type V . . . . .	40
30 - Theoretical versus Experimental Load-Deflection Curves for Aluminum Web-Stiffened Panel-Type VI . . . . .	41
31 - Theoretical versus Experimental Load-Deflection Curves for Aluminum Web-Stiffened Panel-Type VII . . . . .	42
32 - Theoretical versus Experimental Load-Deflection Curves for Aluminum Web-Stiffened Panel-Type VIII . . . . .	43
33 - Underbody of SK-5 following Impact on an Ice Obstacle during 1971 SEV Arctic Trials . . . . .	45
34 - Vertical Kinetic Energy of 150- and 540-Ton ASEV's as a Function of Impact Velocity . . . . .	47
35 - Energy-Absorbing Capacity versus Scale Factor . . . . .	49
36 - Weight of Collision Protection System as a Function of Maximum Impact Velocity . . . . .	50
37 - Weight of Collision Protection System as a Function of Allowable Impact Velocity . . . . .	52

## ABSTRACT

The impact behavior of stiffened and unstiffened square aluminum panels under fixed boundary conditions was investigated experimentally and theoretically, and the ultimate energy-absorbing characteristics were determined as a function of geometry. The effect of rigid, closed-cell foam (2-lb/ft<sup>3</sup> urethane) on an unstiffened panel was also investigated. A geometric scaling law was developed to extrapolate experimental results to sizes needed for the underbody collision protection system of surface effect vehicles for Arctic operation. Protection levels were determined as a function of allowable vertical impact velocity and craft weight.

## ADMINISTRATIVE INFORMATION

This experimental work was funded by the Advanced Research Projects Agency (ARPA) under Order 1676, Program Code ON10, and administered by the Arctic Surface Effect Vehicle Program Office at the Naval Ship Research and Development Center (NSRDC). Preparation of this report was funded by the Naval Sea Systems Command (NAVSEA 035) under Task Area SF 43.422.703-12, Task 17934, Structures for High Performance Ships.

## INTRODUCTION

Surface effect vehicles (SEV) have recently been proposed for operational use in the hostile environment of the Arctic. Vehicles intended for such use are designated ASEV's. They will have the capability of attaining high speeds while operating over water and irregular ice terrain. They are expected to encounter a variety of adverse weather conditions which could well challenge their capability to detect and avoid obstacles. For instance, a craft must be able to climb slopes and pass over objects such as ice ridges, hummocks, and ice pinnacles at high speeds. This is depicted in Figure 1 for a 10-ton ASEV.<sup>1</sup> Any loss of power to the lift system could cause the vehicle to descend onto an ice obstacle; if the velocity were sufficient, the resulting impact could cause penetration damage to the craft (Figure 2). The craft could also experience eccentric collisions to its center of gravity, causing it to rotate in pitch or roll.

---

<sup>1</sup>Shabelski, J.J. and R. Putnam, "Summary Report on 1971 Arctic Trials of 10-Ton Surface Effect Vehicle," NSRDC Report 4100 (May 1973).



Figure 1 – 10-Ton ASEV (SK-5) Test Craft Navigating an Ice Obstacle

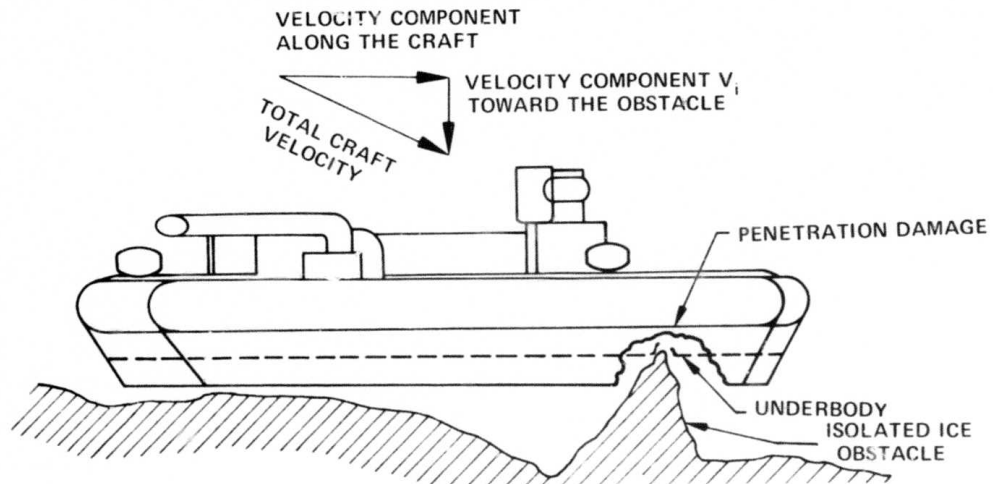


Figure 2 – “Ski Jumping” an Ice Obstacle

Because ice obstacles remain a threat to Arctic operations, the ASEV must be designed to withstand a given impact velocity and resist the penetration of ice obstacles through its underbody. Unless this can be accomplished, the operational capabilities of such craft could be restricted.

This study starts with the assumption that a collision will occur and that the underbody must be designed to sustain such loading without rupture. One concept in underbody

protection is that of utilizing the underbody plating as a "skid pan." This structure would direct the craft past an obstacle while absorbing the energy component toward the obstacle without rupturing. The problem of course, is to design the plating to prevent obstacle penetration for the energy of the vertical collisions. In the "skid pan" approach, only the impact energy in the vertical direction is considered. There is far more kinetic energy in the direction along the craft underbody since the craft velocity in that direction is much higher than the vertical velocity. By utilizing the "skid pan" approach, the large kinetic energy component along the craft underbody need not be considered, vertical deflections must be small, however. Three possible modes of damage define the possible collision scenario:

1. The plating crushes the ice obstacle under dynamic compressive loading with no plastic deformation (permanent set) in the plating.
2. Both the plating and the ice obstacle deform.
3. The plating deforms plastically but the ice obstacle remains rigid.

In Case 1, the damage is to the ice obstacle and therefore underbody collision is not a problem. Case 2 is unlikely for high energies since ice is brittle. If the plating in Case 2 deforms without rupturing, Case 2 quickly degenerates to either Case 1 or 3 except in the unlikely event that the crush loads of the ice and the structure are identical. Case 3, then, is the only case of concern because it is the only one that causes damage to the craft.

It is the goal of this phase of the ASEV collision program to provide design guidelines for energy-absorbing structure. This report documents the experimental investigation of the energy-absorbing capability of stiffened and unstiffened square aluminum panels with fix end boundary conditions.

The particular goal of this program is to determine the feasibility of protecting the craft against vertical impact velocities of 3 to 5 ft/sec. To assist in this determination, a geometric scaling law is derived and used to scale panels from the sizes used in experimental investigations to those reasonable for 150- and 540-ton ASEV's.

## EXPERIMENTAL DETERMINATION OF PANEL RESPONSE

### EXPERIMENTAL SETUP

A series of drop tests was conducted utilizing a 50-ft drop tower (Figure 3) and a panel test fixture (Figure 4). Impact was attained by dropping an 812.6-lb weight from various heights to rupture a given panel. The impact head was positioned to collide in the center of the test panel, and the impacting mass was released from the desired height by means of an electrical solenoid mechanism. A 6-in.-diameter hemispherical head (HY-80 steel) was welded

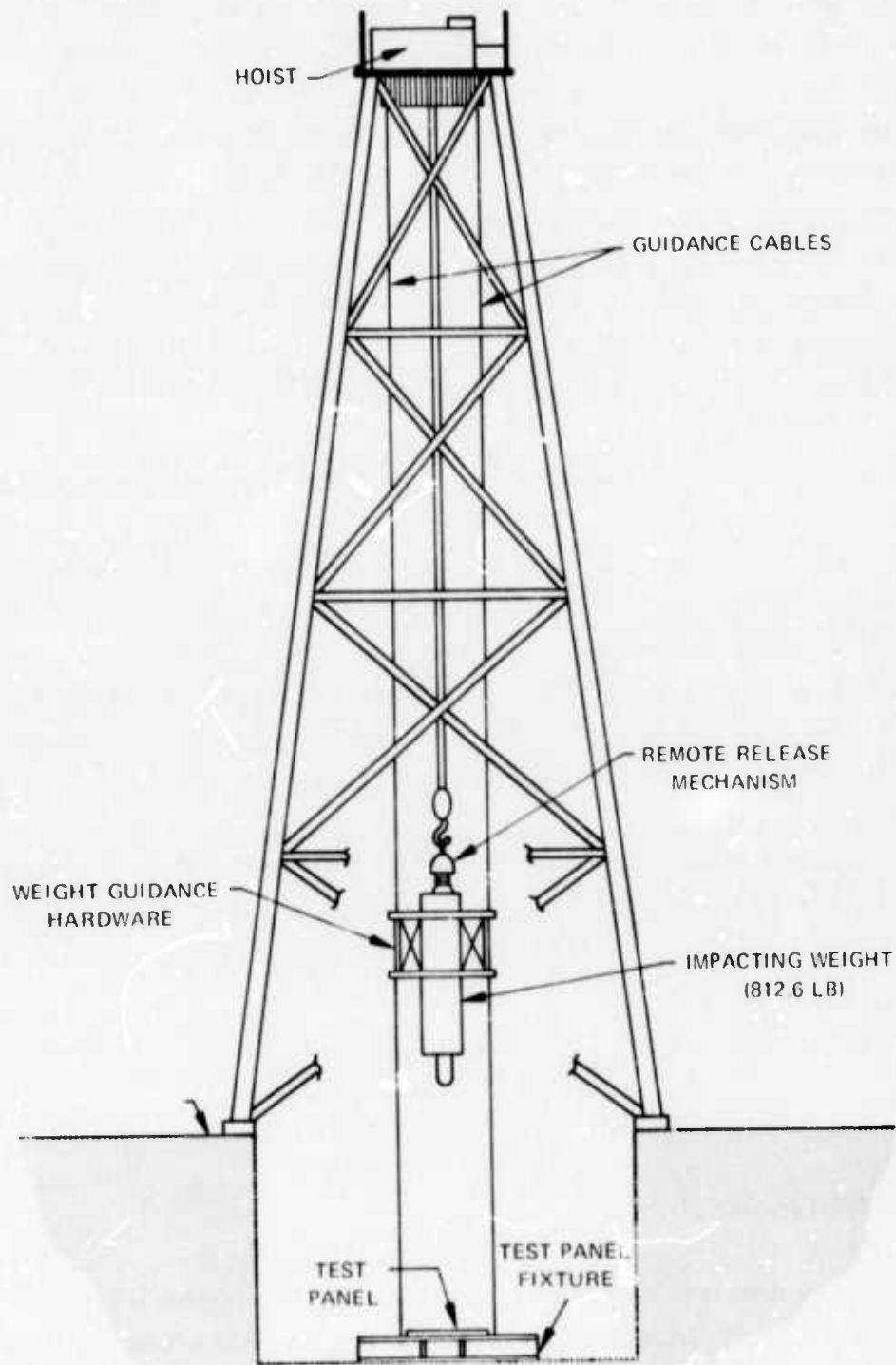


Figure 3 - NSRDC Drop Test Tower Facility

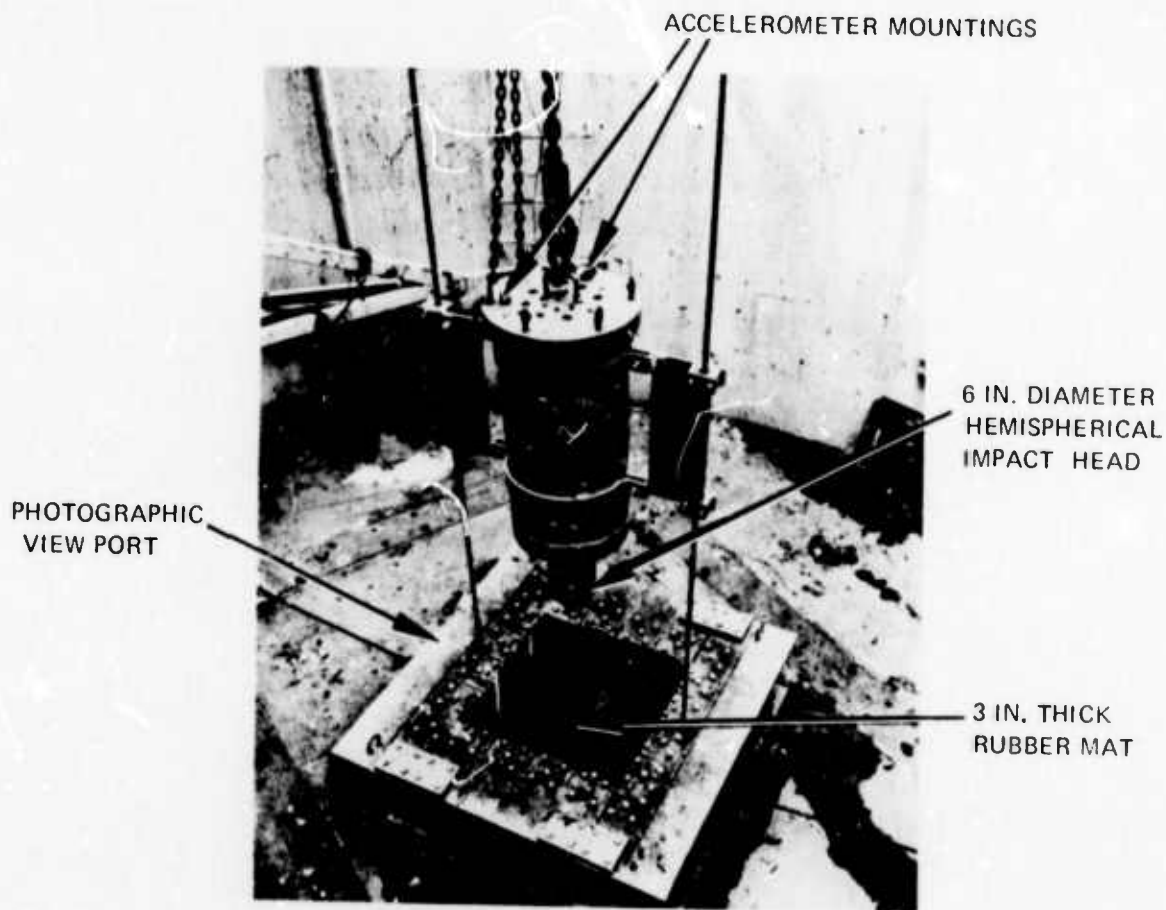


Figure 4 – Panel Testing Fixture

to the bottom of the impact weight to simulate a nonyielding ice object. A 3-in.-thick rubber mat was placed on the nonyielding foundation to protect the instrumentation from exceeding design limits during the impact.

The test fixture (Figure 4) consisted of four steel I-beams rigidly connected to form an open box; the box was positioned between the guide cables of the drop tower and bolted to the foundation. The test fixture is capable of accepting both stiffened and unstiffened panels as large as 30 X 30 in. (24 X 24 in. effective panel area). Slots are provided in the top flanges of the test fixture for installation of stiffened panels. Panels are bolted to the test fixture and clamped on all four edges.

## INSTRUMENTATION

Accelerometers were positioned on the impacting weight to determine the accelerations (decelerations) along the line of impact. Two accelerometers were used to reduce the

possibility of loss of data and to evaluate and increase the accuracy of the system. Data from the accelerometers were amplified, recorded on magnetic tape, and later printed by using an oscillograph.

Since the impacting mass was free falling, the vertical acceleration of gravity acted along the same line as the panel crush forces. Only gravity and the panel crush forces contribute to vertical accelerations, and thus panel crush forces were defined simply by multiplying the measured values by the impacting mass.

Inasmuch as the acceleration data indicate not only crush force but also motion, the data yield acceleration-time information as well as force-deflection information. This allows an evaluation of energy-absorbing capability to rupture for a given panel.

Test panel behavior up to and including rupture was recorded by high-speed photography. A photosonic high-speed camera was located for selected tests as shown in Figure 4. Camera speed was 1000 frames/sec.

## **PANEL GEOMETRY AND FABRICATION**

Test panels were fabricated from 5086-H32 (0.063 and 0.125 in.) aluminum sheets and 5456 H343 (0.125 in.) aluminum sheets. Individual test panels varied in material properties, plate thickness, stiffener thickness, stiffener height, stiffener spacing and stiffener type. Each stiffened panel was welded by using 5356 aluminum filler material. To prevent excess panel distortion during welding, the test plates were spot clamped on each corner and in the middle of all four sides to a 1/4-in. aluminum square backup plate.

## **TEST RESULTS**

### **RESPONSE CHARACTERIZATION**

Test results for selected stiffened and unstiffened panels are given in Figure 5 in the form of acceleration-time histories. Bending response was the most readily detectable difference between responses of various types of panels. It was characterized by a more or less constant acceleration crush force. The unstiffened plates responded primarily in membrane behavior, which was characterized by a more or less linear rise to a peak crush force. This is shown in Figure 6 along with photographs taken at selected time intervals. The slight deviation from the linear acceleration curve during the first 3 msec of response (Figure 6)

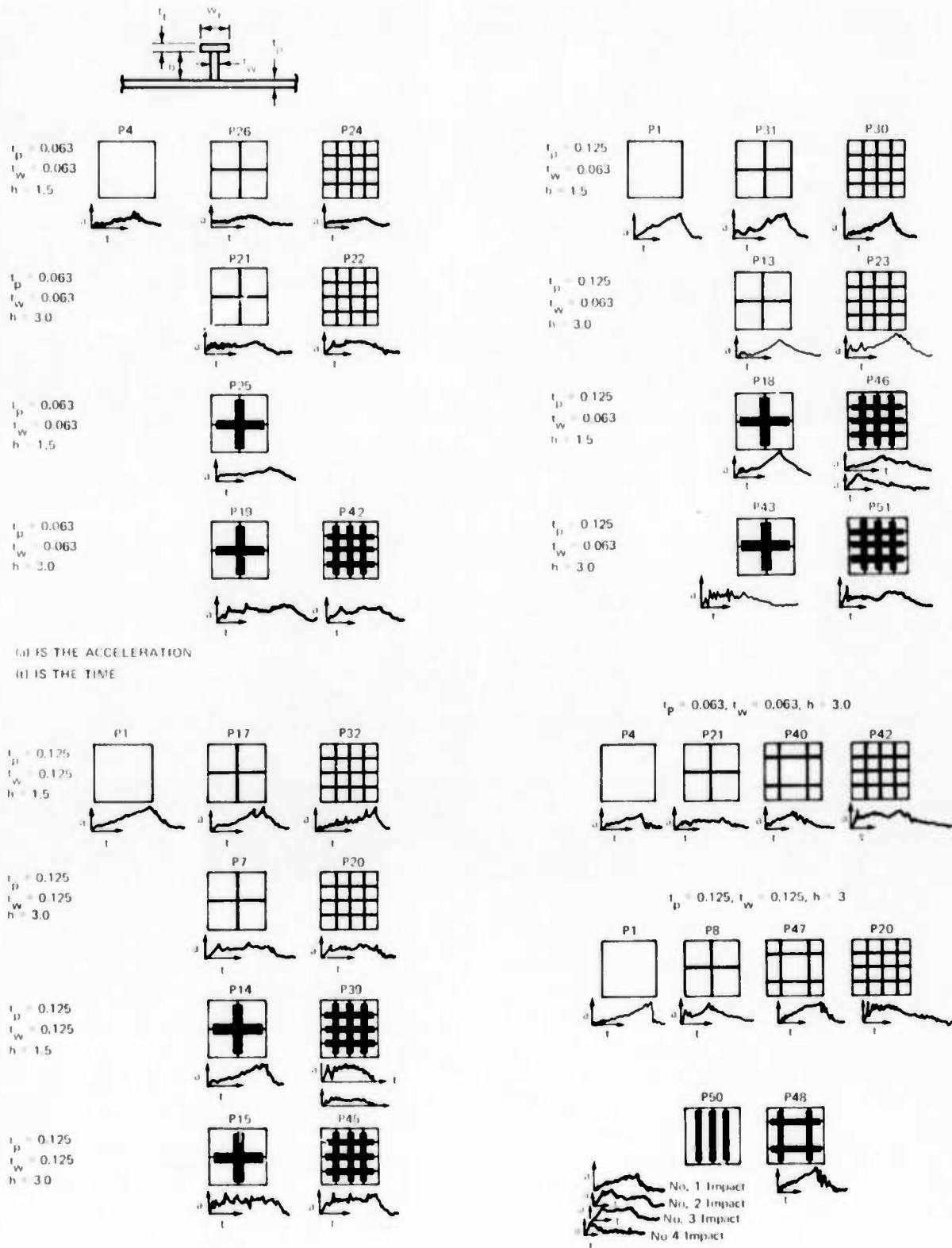
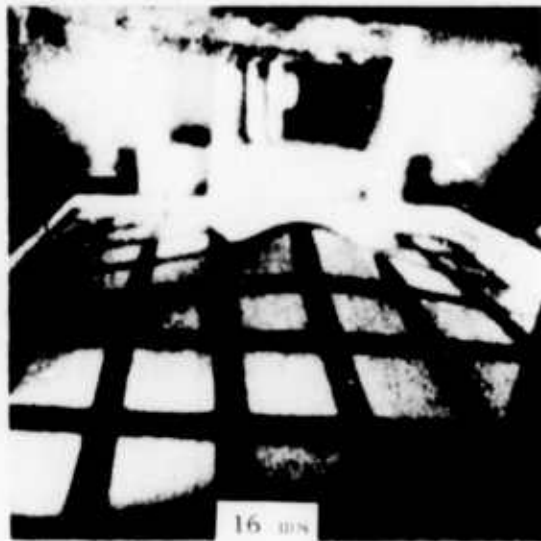
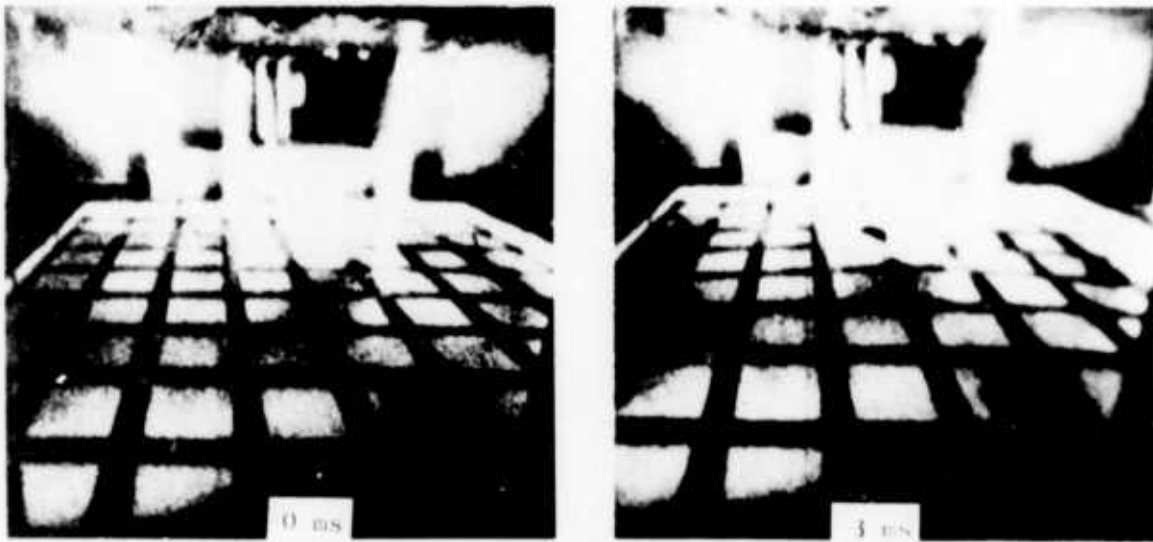


Figure 5 — Characteristic Acceleration-Time Traces for Various Panel Geometries



0.125 IN.  
 TEST P10  
 DROP HEIGHT = 5.0 FT  
 MATERIAL 5086-H32

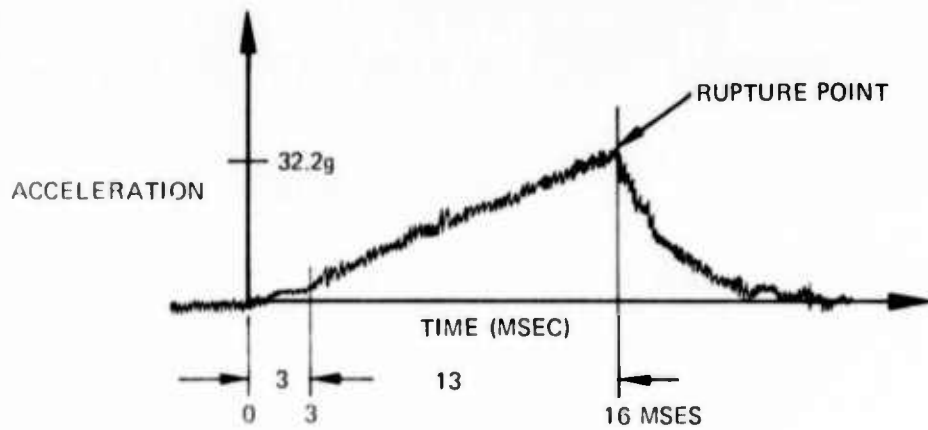


Figure 6 - Acceleration-Time History of Unstiffened Panel

was probably a result of local bending response as the panel conformed to the impact head. Panels with web stiffeners (with and without flanges) for a number of stiffener combinations exhibited both bending and membrane behavior.

The type of response was a function of the geometry of the stiffened panel. For example, a (1 X 1)\* web-stiffened panel (i.e., no flange on the stiffener) with a plate thickness of 0.125 in., web stiffener height of 3.0 in., and web stiffener thickness of 0.125 in. exhibited primarily bending behavior. In contrast, for these same thicknesses of plate and web stiffness, a (1 X 1) web-stiffened panel with a stiffener height of 1.5 in., exhibited primarily membrane behavior. Figure 7 illustrates bending behavior in a particular panel as shown in several frames from high-speed movies of the impact. Note that although the response was primarily bending, there was also some membrane response, particularly at large deformations. Figure 7 shows evidence of buckling of the web stiffener just prior to noticeable membrane behavior. Tearing of the stiffeners along the heat-affected zone at the center intersection may also be seen late in the impact.

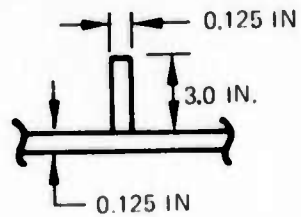
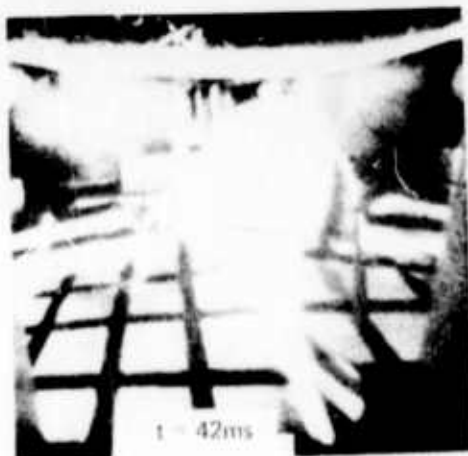
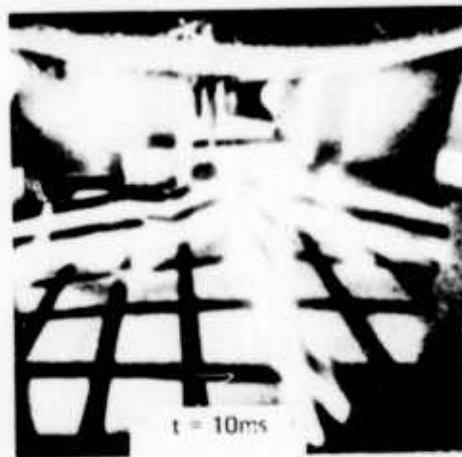
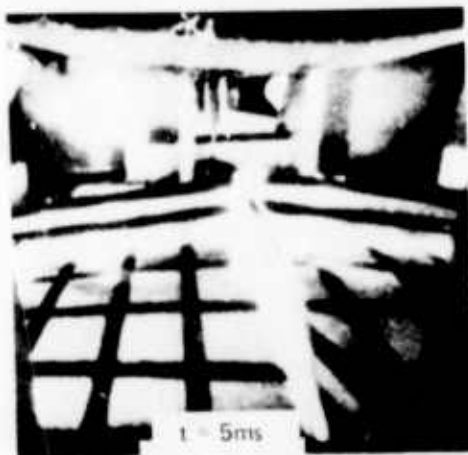
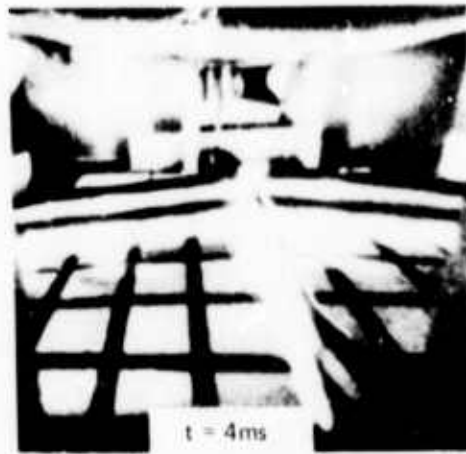
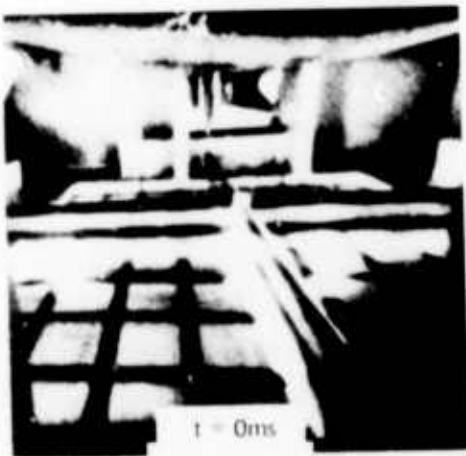
Panels with flanged stiffeners also exhibited both bending and membrane behavior; again, the type of response was a function of panel geometry. A significant difference in the behavior of a flanged-stiffener panel compared to that of a web-stiffened panel was the reduction in web buckling in the former. Figure 8 shows the stiffener rotation or "tripping" that occurred at 10 msec for a (1 X 1) flanged stiffener panel with a plate thickness of 0.125 in., a stiffener height of 1.5 in., a stiffener thickness of 0.125 in., a flange thickness of 0.125 in., and a flange width of 1.0 in. Tearing of the weld of the flange at the center of the panel may also be seen in Figure 8. This particular panel is considered to have displayed primarily membrane behavior. Figure 9 shows a closeup of a weld tearing on a similar panel.

## DATA REDUCTION PROCESS

The accelerometer data were recorded continuously with time and digitized by selecting discrete acceleration and time points. The acceleration data were multiplied by the mass of the impacting cylinder to define crush force for each digitized time point, and the same acceleration data were integrated twice to each point to define a displacement corresponding

---

\* This notation is used throughout this report and indicates that one stiffener is oriented in each direction of the plane of the panel. That is, an (M X N) panel refers to a panel stiffened by M stiffeners in one direction and N stiffeners in the orthogonal direction.



TEST P8  
DROP HEIGHT = 6.0 FT  
MATERIAL 508G-H32

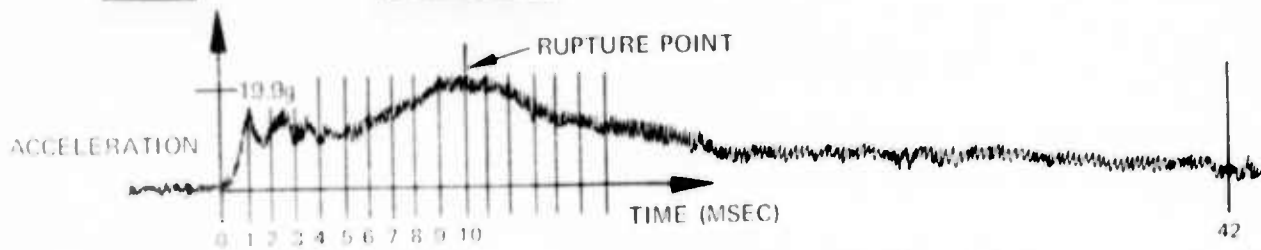
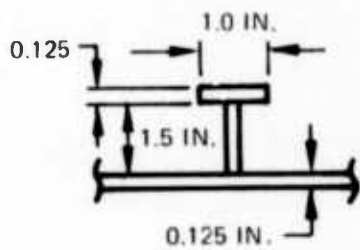
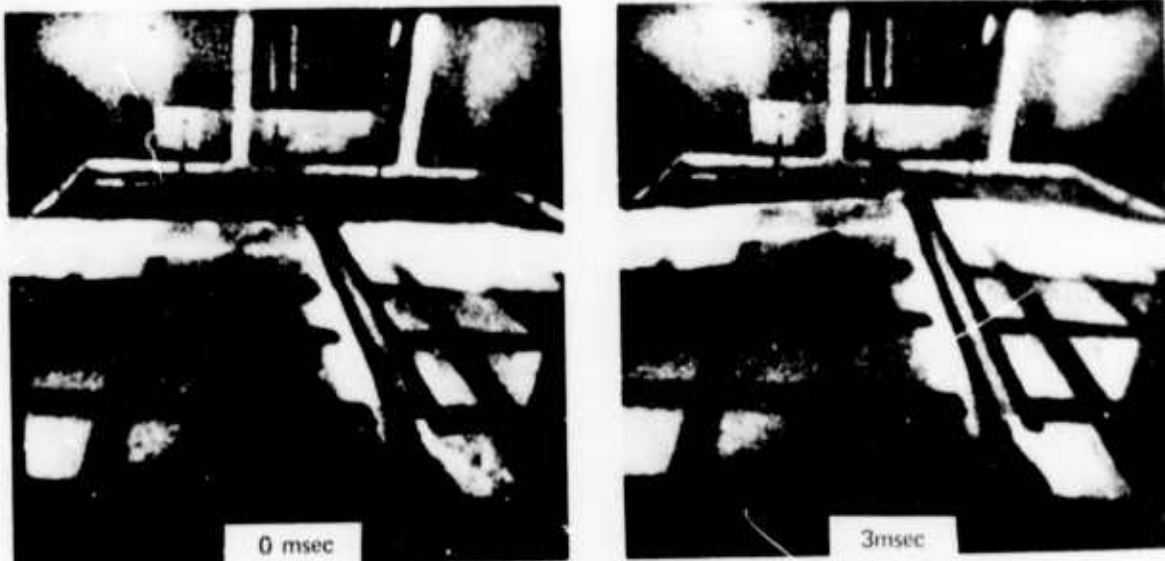


Figure 7 - Acceleration-Time History of Web-Stiffened Panel



TEST P14  
 DROP HEIGHT = 6.0 FT  
 MATERIAL 5086-H32

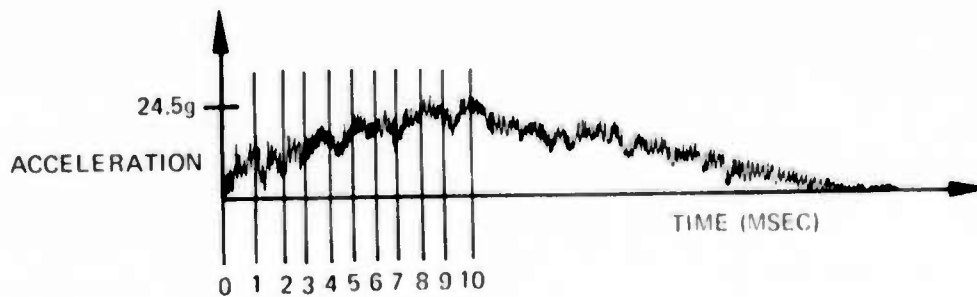
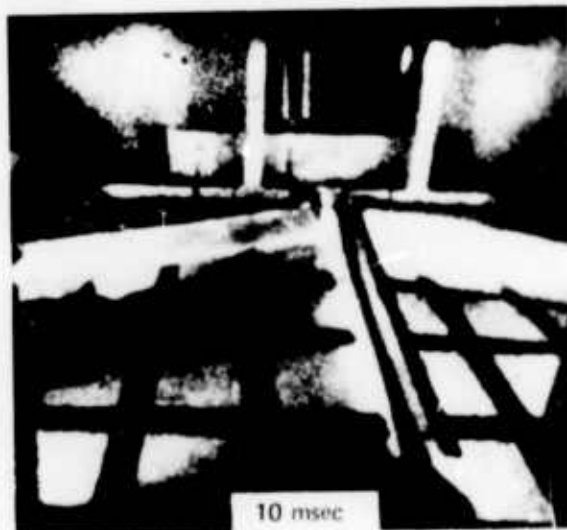


Figure 8 - Acceleration-Time History of Panel with Flanged Stiffeners

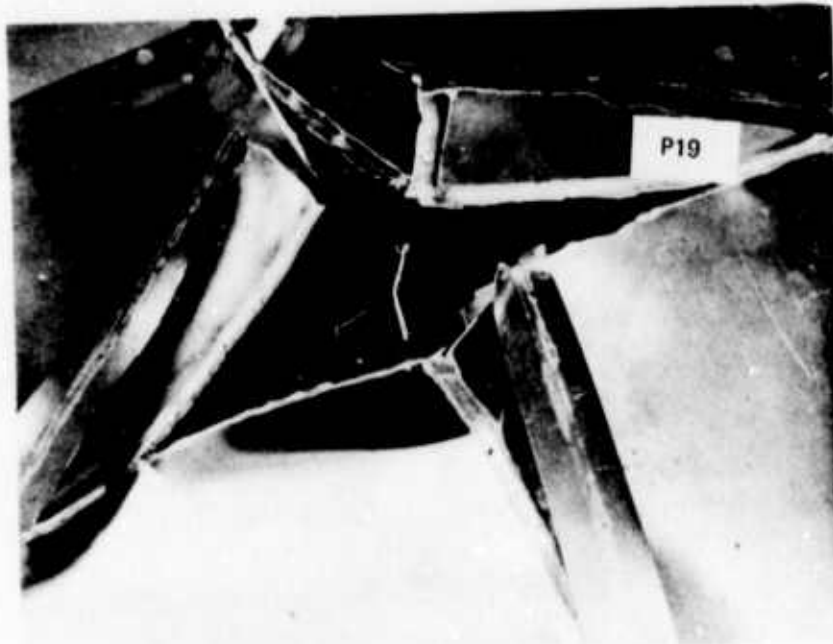


Figure 9 – Closeup of Welding Failure in the Heat-Affected Zone

to each digitized time point. The free-fall acceleration data immediately prior to impact serve as a reference acceleration, namely, the acceleration of gravity. Deflection is considered to be zero at the time of initial contact.

A numerical integration computer program was written to calculate collision motions and energy absorption. Figure 10 indicates the test data used as input to the computer program, and Figure 11 is a sample of computer output. The velocity-time history is simply the integrated acceleration with an initial velocity of the calculated free-fall velocity at the time of initial contact. Since the load-time history and the displacement-time history are both defined, the load-displacement curves are also defined. The energy absorbed is simply the integration of the load-displacement curve and is shown in Figure 11 as well.

### ENERGY ABSORPTION

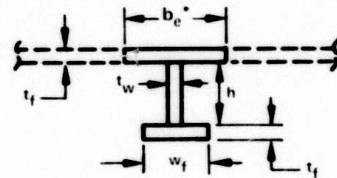
The amount of energy a panel can absorb depends on its load-deflection curve. The energy-absorbing capability of a panel is the integration of the load-deflection curve to the deflection at rupture. The energy absorbed at any intermediate deflection is simply the integration to the deflection. The crush forces in any collision are defined by the dynamic load-deflection relationship, which for the stiffened and unstiffened aluminum panels is simply the static load-deflection curve.

Figure 10 – Test Data Used for Computer Program

Test Number	Drop Height ft	Material	t <sub>D</sub> in.	t <sub>w</sub> in.	h in.	b <sub>w</sub> in.	t <sub>1</sub>	w <sub>1</sub>	Form	Acceleration Peak ft/sec <sup>2</sup>	Deflection (W) in.	Energy Absorbed at Rupture ft-lb
P 1	5	5086 H32	0.125	-	-	-	-	-	Plate	1002	2.87	2655
2	5	5086 H32	0.125	-	-	-	-	-	Plate	1048	2.68	2894
3	5	5456 H343	0.125	-	-	-	-	-	Plate	1138	2.61	2606
4	4	5086 H32	0.063	-	-	-	-	-	Plate	399	1.86	801
5	4	5086 H32	0.063	-	-	-	-	-	Plate	426	1.67	816
6	8	5456 H343	0.125	0.125	3	3.96	-	-	1 X 1	598	1.79	1730
7	6	5456 H343	0.125	0.125	3	3.96	-	-	1 X 1	1002	2.26	2413
8	6	5086 H32	0.125	0.125	3	4.79	-	-	1 X 1	642	2.26	520
9	6	5456 H343	0.125	0.125	1.5	3.96	-	-	3 X 3	725	2.18	1965
10	5	5086 H32	0.125	-	-	-	-	-	-	1036	3.07	3001
11	4	5086 H32	0.125	0.125	1.5	4.79	-	-	1 X 1	631	2.47	2170
12	4	5086 H32	0.125	0.063	3	4.79	-	-	1 X 1	825	3.03	2557
13	5	5086 H32	0.125	0.063	3	4.79	-	-	1 X 1	850	2.69	2336
14	6	5086 H32	0.125	0.125	1.5	-	0.125	1.0	1 X 1 WF	790	3.01	2427
15	6	5086 H32	0.125	0.125	3	-	0.125	2.0	1 X 1 WF	478	3.29	4293
16	6	5456 H343	0.125	0.125	1.5	-	0.125	1.0	1 X 1 WF	893	2.41	2630
17	5	5456 H343	0.125	0.125	1.5	3.96	-	-	1 X 1	688	2.15	2020
18	6	5086 H32	0.125	0.063	1.5	-	0.063	1.0	1 X 1 WF	970	2.96	2849
19	6	5086 H32	0.063	0.063	3	-	0.063	2.0	1 X 1 WF	260	2.20	1349
20	7	5456 H343	0.125	0.125	3	3.96	-	-	3 X 3	766	1.71	2460
21	4	5086 H32	0.063	0.063	3	2.42	-	-	1 X 1	195	2.48	1162
22	4	5086 H32	0.063	0.063	3	2.42	-	-	3 X 3	275	1.72	914
23	5	5086 H32	0.125	0.063	3	4.79	-	-	3 X 3	760	2.17	2022
24	4	5086 H32	0.063	0.063	1.5	2.42	-	-	3 X 3	2693	2.08	883
25	3	5086 H32	0.063	0.063	1.5	-	0.063	1.0	1 X 1 WF	293	2.67	976
26	3	5086 H32	0.063	0.063	1.5	2.42	-	-	1 X 1	275	1.83	666
27	4	5456 H343	0.125	-	-	-	-	-	Plate	1106	2.81	2902
28	6	5456 H343	0.125	0.125	3	3.96	-	-	3 X 3	783	1.71	2283
29	6	5456 H343	0.125	0.125	3	3.96	-	-	3 X 3	416	1.85	2227
30	4	5086 H32	0.125	0.063	1.5	4.79	-	-	3 X 3	609	2.27	1637
31	4	5086 H32	0.125	0.063	1.5	4.79	-	-	1 X 1	586	2.61	1765
32	4	5086 H32	0.125	0.125	1.5	4.79	-	-	3 X 3	670	2.26	1997
33	4	5086 H32	0.063	0.063	1.5	-	0.063	1.0	3 X 3 WF	Bad Data		
34(1)	4	5086 H32	0.125	0.063	3	-	0.063	2.0	3 X 3 WF	567	3.01	3450
34(2)	2	5086 H32	0.125	0.063	3	-	0.063	2.0	3 X 3 WF	-	-	387
34	4/2	5086 H32	0.125	0.063	3	-	0.063	2.0	3 X 3 WF	-	-	3837
35(1)	5	5456 H343	0.125	-	-	-	-	-	Plate-Foam 5.75"	980	7.30	4530
35(2)	3	5456 H343	0.125	-	-	-	-	-	Plate-Foam 5.75"	-	-	154
35	5/3	5456 H343	0.125	-	-	-	-	-	Plate-Foam 5.75"	-	-	4684
36	7	5086 H32	0.125	-	-	-	-	-	Plate-Foam 5.75"	-	-	4715
37	4	5086 H32	0.063	-	-	-	-	-	Plate-Foam 5.75"	484	3.95	1699
38	4	5086 H32	0.063	0.063	1.5	2.42	0.063	1.0	3 X 3 WF-Foam 5.75"	344	6.41	1648

Figure 10 (Continued)

Test Number	Drop Height ft	Material	$t_p$ in.	$t_w$ in.	h in.	$t_e$ in.			Form	Acceleration Peak ft/sec <sup>2</sup>	Deflection (W) in.	Energy Absorbed at Rupture ft-lb
39(1)	6	5456 H343	0.125	0.125	1.5		0.125	1.0	3 X 3 WF	534	3.17	3,794
39(2)	3	5456 H343	0.125	0.125	1.5		0.125	1.0	3 X 3 WF			282
39	6/3	5456 H343	0.125	0.125	1.5		0.125	1.0	3 X 3 WF			4,076
40	4	5086 H32	0.063	0.063	3		-	-	2 X 2	407	1.57	828
41	4	5086 H32	0.063	0.063	1.5	4.79	-	-	3 X 3	Bad Date		
42	4	5086 H32	0.063	0.063	3		0.063	2.0	3 X 3 WF	440	2.04	1,933
43	7	5456 H343	0.125	0.125	3		0.125	2.0	1 X 1 WF	397	3.38	4,119
44	5	5086 H32	0.063	0.063	1.5		0.063	1.0	3 X 3 WF		Bad Data	
45(1)	8	5086 H32	0.125	0.125	3		0.125	2.0	3 X 3 WF	1045	1.00	3,285
45(2)	5	5086 H32	0.125	0.125	3		0.125	2.0	3 X 3 WF			2,318
45(3)	4	5086 H32	0.125	0.125	3		0.125	2.0	3 X 3 WF			599
45	8 5 4	5086 H32	0.125	0.125	3		0.125	2.0	3 X 3 WF			6,202
46(1)	4	5086 H32	0.125	0.063	1.5		0.063	1.0	3 X 3 WF	421	3.49	3,473
46(2)	3	5086 H32	0.125	0.063	1.5		0.063	1.0	3 X 3 WF			205
46	4/3	5086 H32	0.125	0.063	1.5		0.063	1.0	3 X 3 WF			3,678
47	5	5086 H32	0.125	0.125	3		-	-	2 X 2	1017	2.37	2,976
48	5	5086 H32	0.125	0.125	3		0.125	2.0	2 X 2 WF	1104	2.42	2,766
49(1)	5	5086 H32	0.125	0.125	1.5		0.125	1.0	3 X 3 WF	974	2.61	3,605
49(2)	4	5086 H32	0.125	0.125	1.5		0.125	1.0	3 X 3 WF			335
49	5 4	5086 H32	0.125	0.125	1.5		0.125	1.0	3 X 3 WF			3,940
50(1)	4	5086 H32	0.125	0.125	3		0.125	2.0	3 X 0 WF	1084	2.30	3,405
50(2)	5	5086 H32	0.125	0.125	3		0.125	2.0	3 X 0 WF			3,697
50(3)	4	5086 H32	0.125	0.125	3		0.125	2.0	3 X 0 WF			2,765
50(4)	4	5086 H32	0.125	0.125	3		0.125	2.0	3 X 0 WF			271
50	4 5 4 4						0.125	2.0				10,128
51	6	5086 H32	0.125	0.063	3		0.063	2.0	3 X 3 WF	664	2.87	3,429



\* Taken as the "effective width of plating" and calculated from page 31.

TEST NUMBER 1

IMPACT TIME HISTORY      IMPACT WEIGHT (LB) IS      812.600  
 DROP HEIGHT (FT) IS      5.000  
 POTENTIAL ENERGY (FT-LB) IS      .40630E+04

TIME (SEC)	ACCELERATION (FT/SEC-SEC)	VELOCITY (FT/SEC)	DISPLACEMENT (IN.)	ABSORBED ENERGY (FT-LB)
0.	0.	-.17944E+02	0.	0.
.50000E-03	.10980E+02	-.17942E+02	-.10766E+00	.85334E+01
.10000E-02	.21960E+02	-.17933E+02	-.21529E+00	.19549E+02
.15000E-02	.32940E+02	-.17920E+02	-.32285E+00	.33042E+02
.20000E-02	.43920E+02	-.17900E+02	-.43031E+00	.49004E+02
.25000E-02	.54900E+02	-.17876E+02	-.53764E+00	.67425E+02
.30000E-02	.92784E+02	-.17839E+02	-.64480E+00	.91321E+02
.35000E-02	.13067E+03	-.17783E+02	-.75167E+00	.12367E+03
.40000E-02	.16855E+03	-.17708E+02	-.85816E+00	.16438E+03
.45000E-02	.20644E+03	-.17614E+02	-.96413E+00	.21335E+03
.50000E-02	.24432E+03	-.17502E+02	-.10695E+01	.27042E+03
.55000E-02	.28220E+03	-.17370E+02	-.11741E+01	.33543E+03
.60000E-02	.32009E+03	-.17220E+02	-.12779E+01	.40818E+03
.65000E-02	.35797E+03	-.17050E+02	-.13807E+01	.48845E+03
.70000E-02	.39586E+03	-.16862E+02	-.14925E+01	.57598E+03
.75000E-02	.43374E+03	-.16654E+02	-.15830E+01	.67051E+03
.80000E-02	.47162E+03	-.16428E+02	-.16823E+01	.77172E+03
.85000E-02	.50951E+03	-.16183E+02	-.17801E+01	.87929E+03
.90000E-02	.54739E+03	-.15918E+02	-.18764E+01	.99284E+03
.95000E-02	.58528E+03	-.15635E+02	-.19711E+01	.11120E+04
1.0000E-01	.62316E+03	-.15333E+02	-.20640E+01	.12364E+04
1.0500E-01	.66104E+03	-.15012E+02	-.21550E+01	.13655E+04
1.1000E-01	.69893E+03	-.14672E+02	-.22441E+01	.14989E+04
1.1500E-01	.73681E+03	-.14313E+02	-.23311E+01	.16360E+04
1.2000E-01	.77470E+03	-.13935E+02	-.24158E+01	.17765E+04
1.2500E-01	.81258E+03	-.13538E+02	-.24983E+01	.19196E+04
1.3000E-01	.85048E+03	-.13123E+02	-.25782E+01	.20649E+04
1.3500E-01	.88835E+03	-.12688E+02	-.26557E+01	.22118E+04
1.4000E-01	.92623E+03	-.12234E+02	-.27305E+01	.23595E+04
1.4500E-01	.96412E+03	-.11762E+02	-.28025E+01	.25075E+04
1.5000E-01	1.0020E+04	-.11270E+02	-.28716E+01	.26550E+04

END OF TEST NUMBER 1

Figure 11 - Typical Computer Printout of Panel Response

## Effect of Panel Geometry

The energy a given panel can absorb is governed by its geometry. Figure 12 illustrates the characteristic behavior for each panel geometry and the total energy absorbed by the panel. The panel behavior is divided into three types: primarily membrane, transition zone (i.e., both membrane and bending for identical geometries), and primarily bending. The effects of geometry on the energy-absorbing capability of the stiffened and unstiffened panels tested is summarized as follows:

1. Unstiffened (0.063-in. plate thickness) panels respectively absorbed 1.21 and 0.70 times the energy absorption at rupture of (1 X 1) 1.5- and 3.0-in. web-stiffened panels of the same plate thickness.

2. Unstiffened (0.125-in. plate thickness) panels absorbed an average of 1.29 times the energy absorption at rupture of (1 X 1) web stiffened panels of the same plate thickness, and 1.33 times the energy absorption at rupture of (3 X 3) stiffened panels of the same plate thickness.

This is probably due to the fact that welding the stiffeners creates "weak links" where tearing can begin and the panel ruptures before full advantage can be taken of the added strength of the stiffeners and the membrane strength of the plating.

3. The addition of flanges to most web-stiffened geometries significantly increased the energy-absorbing capability of the panel. This is partially a result of an increase in the stiffness of the panel, but—perhaps more important—the additional material was added at the location where the tearing begins and therefore it delayed the initiation of the panel failure. Panels with flanged stiffeners generally exhibited greater energy-absorbing capabilities than unstiffened panels of the same plate thickness.

4. When the impact occurred on a stiffened panel but not directly on a stiffener (Figure 13) the limited available test data indicate that the panel responds as if it were an unstiffened panel of reduced size.

Although the energy-absorbing capability of a given panel is important, the energy absorption per pound of material (specific energy absorption) is also important in weight-sensitive structures like ASEV's. A (3 X 0) stiffened panel showed the highest specific energy absorption (932 ft-lb/lb). This 0.125-in. plate is 5080-H32 with a stiffener height of 3.0 in., stiffener thickness of 0.125 in., flange thickness of 0.125 in. and flange width of 2.0 in. (Figure 14). The specific energies for all the panel geometries tested are presented in Figure 15.



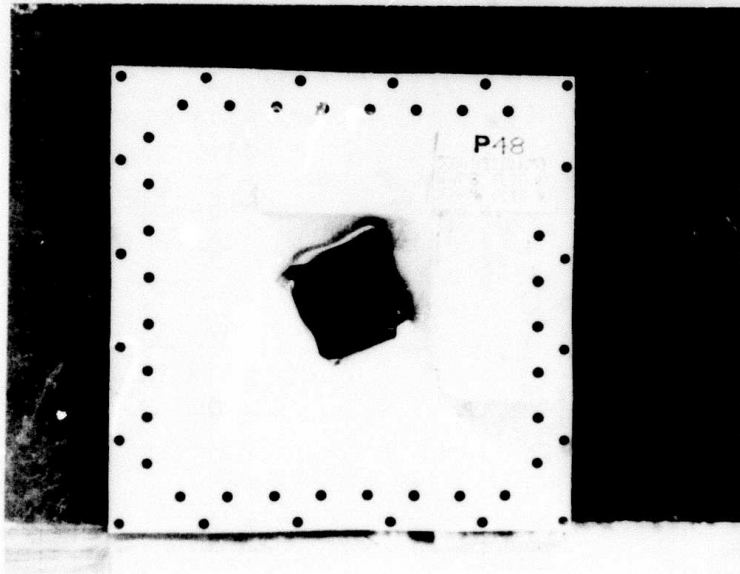
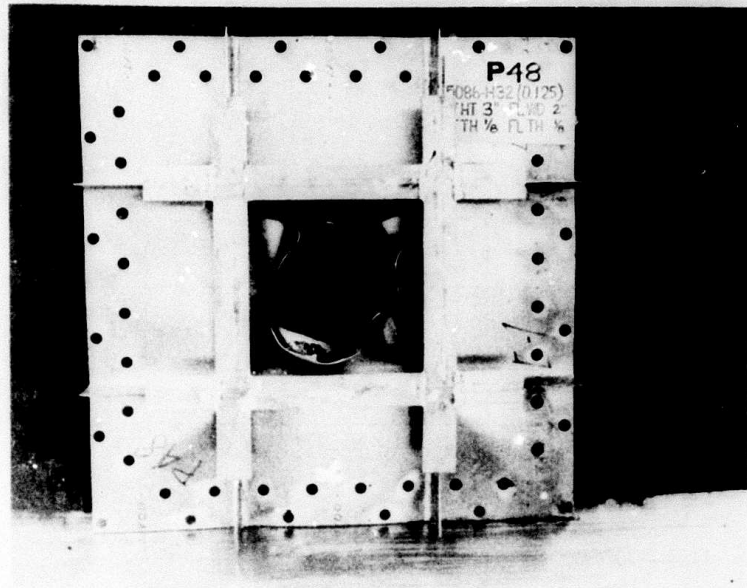


Figure 13 – (2 X 2) Panel with Flanged Stiffeners  
after Impact

(Impact occurred on the panel but not directly on a stiffener)

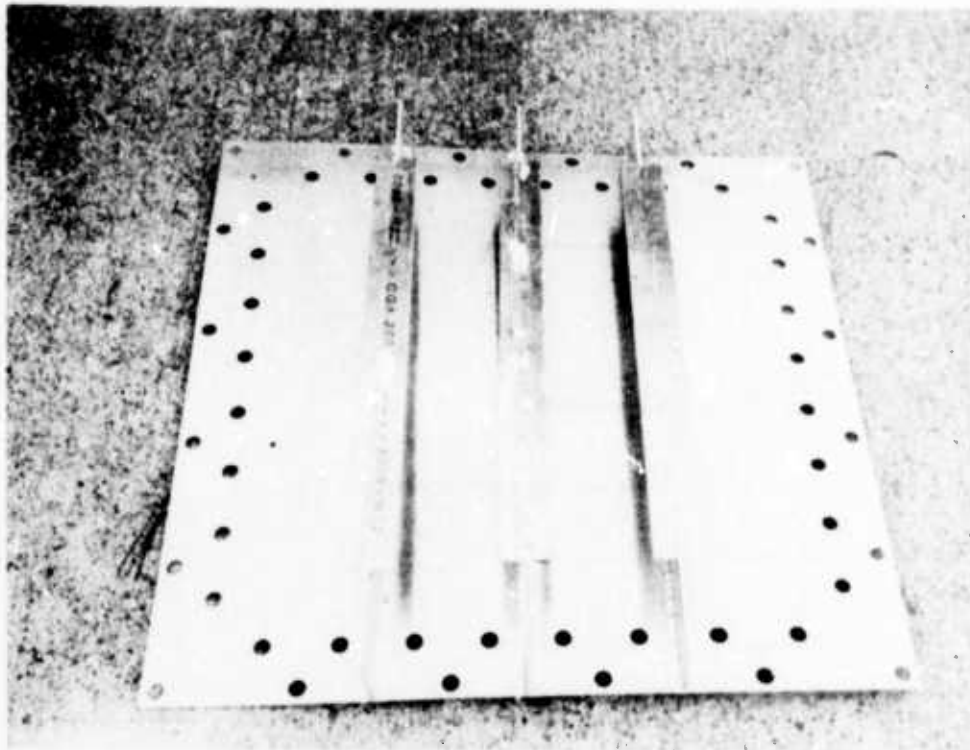
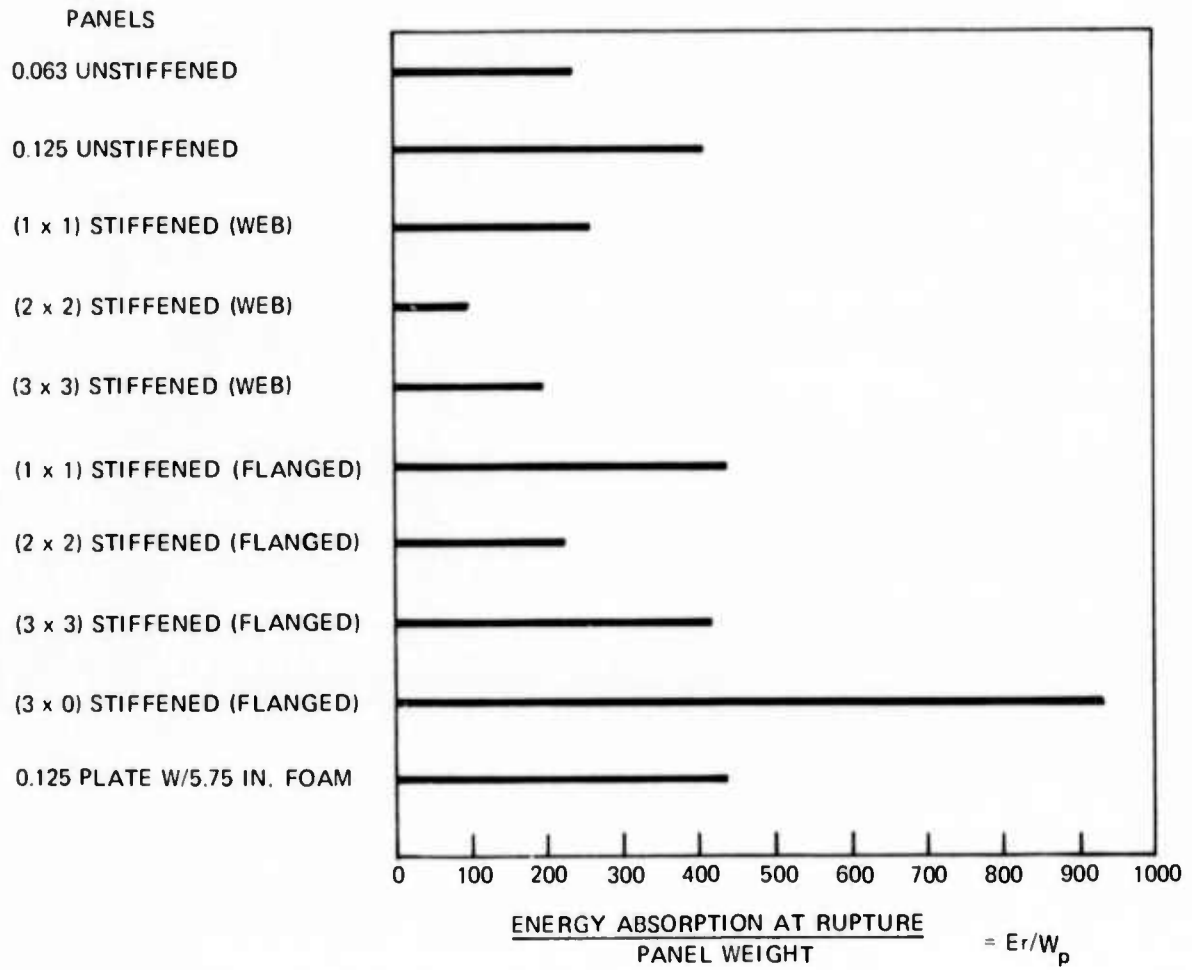


Figure 14 – (3 x 0) Panel with Flanged Stiffeners before Impact



NOTE: ALL STIFFENED PANELS WERE 0.125-IN. MATERIAL WITH  
3.0-IN. HIGH WEB STIFFENERS

Figure 15 – Specific Energy Absorption for Selected Test Series

### Effect of Repeated Loading

Experimental determination of energy-absorbing capability necessitated subjecting some panels to more than one impact. Data from successive impacts were combined to define the total energy-absorbing capability. The procedure is demonstrated for a particular panel which required four successive impacts to rupture. After the first impact (Figure 16a) the center of the panel showed limited permanent set. Evidence of plate tearing did not occur until the second impact (Figure 16b). At this point, however, complete rupture did not occur, and the panel was able to absorb additional energy. It was not until the fourth impact that complete rupture occurred (Figure 16d).

When more than one impact is needed to rupture the test panel and it is thus necessary to sum the additional energy absorbed in each impact, care must be taken not to add energy absorbed through elastic reloading and elastic unloading. The elastic loading energy is included in the first impact since if the panel were impacted to rupture in a single collision, the elastic energy would be a portion of the total energy-absorbing capability. Figure 17 illustrates the portion of the energy absorbed in each impact to be included in the summation. It is interesting to note that the beginning of the plastic range in each successive impact is at the load level of the previous unloading point.

The two types of panel impacts were investigated: (1) those at the center of an unstiffened panel or where the obstacle contacts midway between stiffeners and (2) those where the obstacle impacts directly on a stiffener or at the point of intersection of stiffeners. These cases are studied as bounds on the range of possible panel impacts.

### Effect of Energy-Absorbing Foam

Tests were performed on the combined energy-absorbing capability of a 5.7-in.-thick layer of low density ( $2\text{-lb/ft}^3$ ) urethane foam on a 0.125-in.-thick unstiffened aluminum panel (Figure 18). The foam<sup>2</sup> was cut to the effective size of the panel and encased in a plywood frame to simulate the effect of an infinite layer of foam.

The addition of the foam layer increased the average energy-absorbing capability of unstiffened panels by 84 percent. A single test utilizing foam on a stiffened panel showed a comparable increase (102 percent) in energy-absorbing capability.

---

<sup>2</sup>Furio, A. and W.E. Gilbert, "Impact Test of Urethane Foam," NSRDC Report 4254 (Jan 1974).



Figure 16a – Impact Energy = 3405 Foot Pounds



Figure 16b – Impact Energy = 3695 Foot Pounds

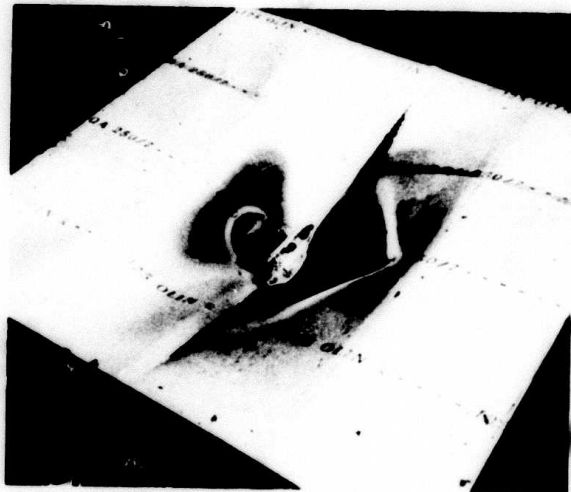


Figure 16c – Impact Energy = 2765 Foot Pounds



Figure 16d – Impact Energy = 271 Foot Pounds

Figure 16 – Damage Sustained by a (3 X 0) Panel with Flanged Stiffeners during Successive Impacts

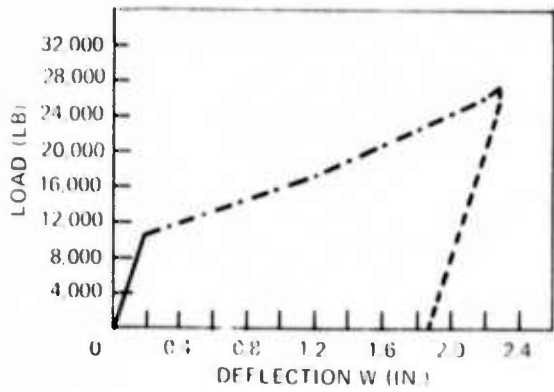


Figure 17a

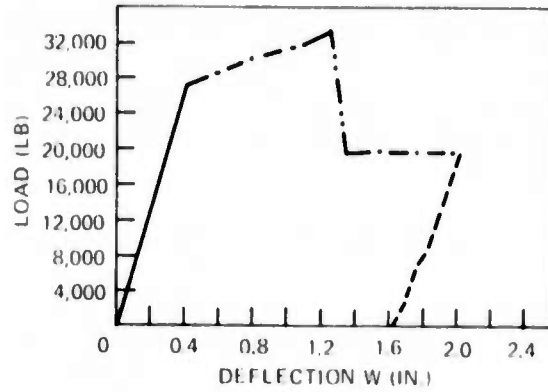


Figure 17b

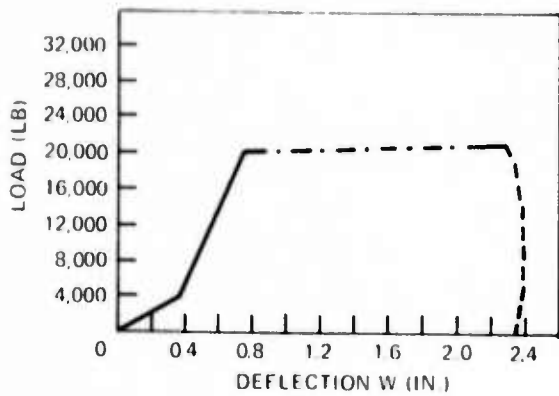


Figure 17c

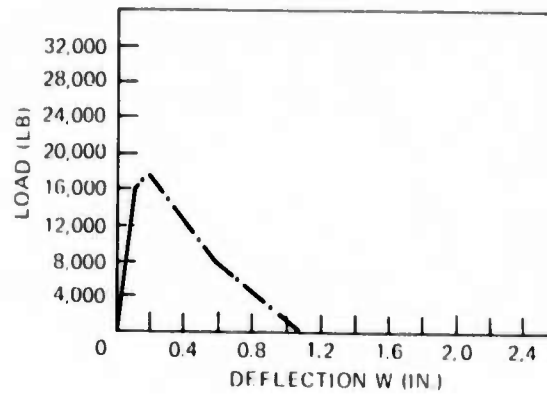


Figure 17d

- ELASTIC RANGE
- - - PLASTIC RANGE
- · · SECONDARY FAILURE
- - - ELASTIC UNLOADING
- · - · RESIDUAL LOAD DEFLECTION

Figure 17 – Load-Deflection Curves for Successive Impacts on a (3 X 0) Panel with Flanged Stiffeners

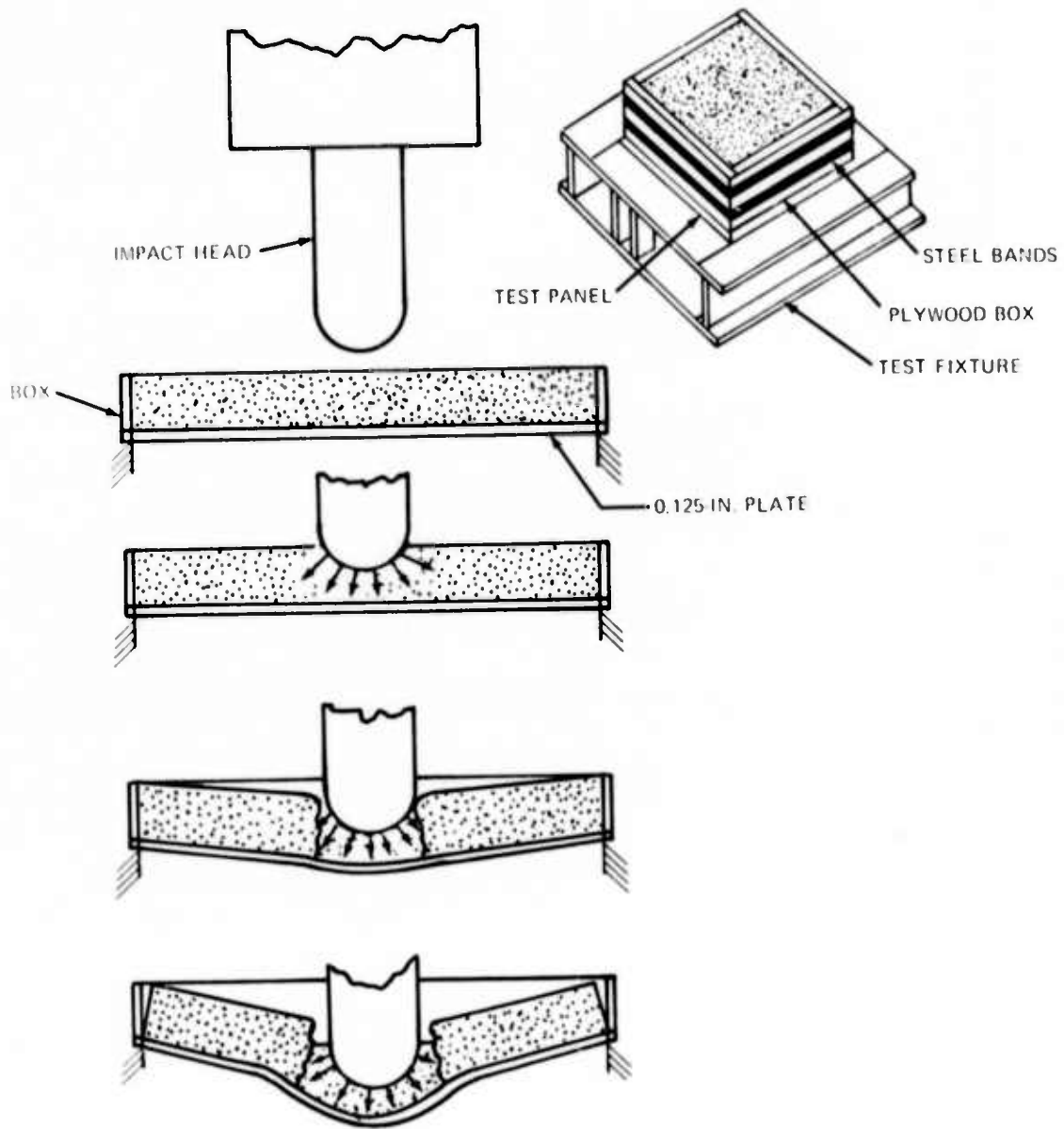


Figure 18 - Response of an Unstiffened Panel with Energy-Absorbing Foam

Figure 19 compares load-time histories of the unstiffened panels with and without the energy-absorbing foam. The panel with foam exhibited a slight increase in peak crush force and a longer load duration. Both effects are most likely due to the load distribution effect of the foam rather than to energy absorbed directly by it. Because of the weight of the foam, however, the specific energy absorption for stiffened and unstiffened panels with a foam layer is comparable to that for the same panel without the foam layer.

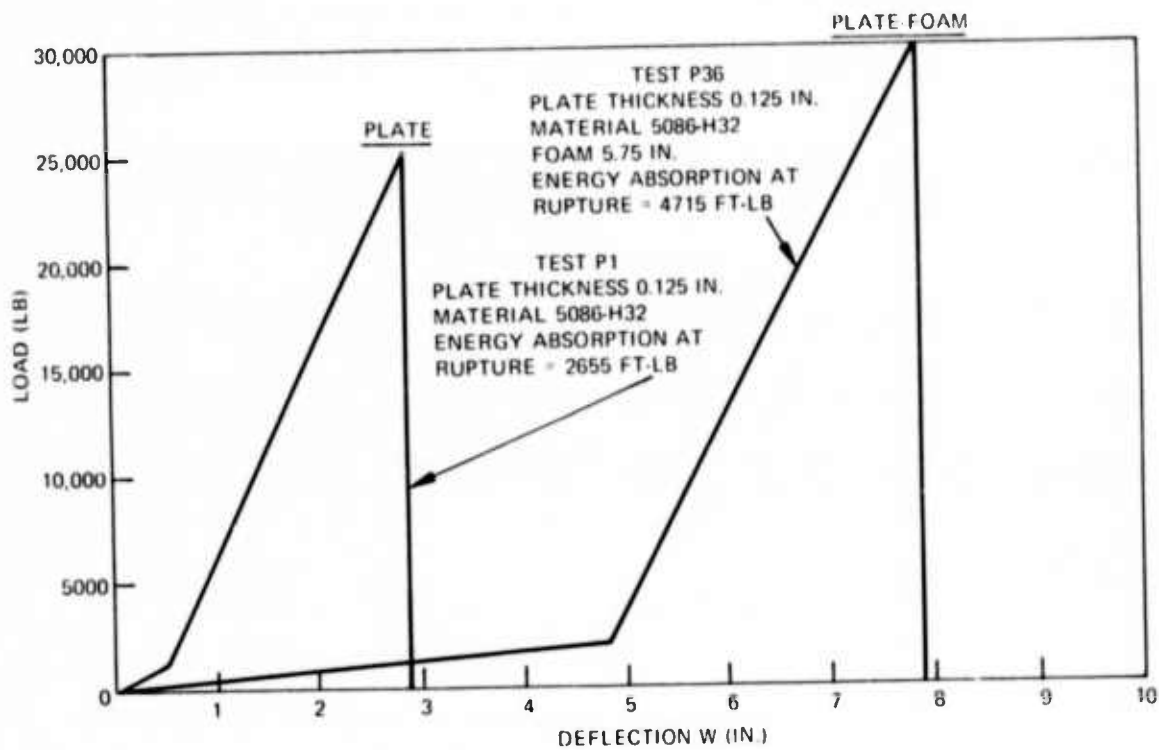


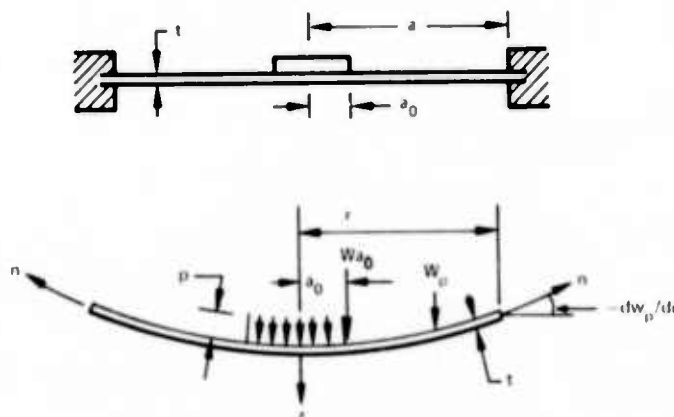
Figure 19 – Comparison of Load-Deflection Curves for a Panel with and without Energy-Absorbing Foam

The shape of the obstacle impacted will probably influence the energy-absorbing characteristics of the foam-panel combination; if the ice obstacle is sharp and pointed, the foam may have little effect.

## THEORETICAL DETERMINATION OF THE LOAD-DEFLECTION CURVES

### UNSTIFFENED SQUARE PLATES

The acceleration-time histories show that unstiffened square plates exhibit primarily membrane behavior to the point of rupture. The following derivation relates the membrane deflection of an unstiffened panel to the applied load. The membrane behavior of a square panel is described by first approximating the square panel by a circular panel of diameter equal to the length of one side of the square panel. The circular panel is statically loaded, as shown in Figure 20, to approximate the impact load. This free-body diagram of the panel illustrates the equilibrium forces and deflections for a panel segment of radius  $r$ , where  $r$  is the distance from the center of the panel in the radial direction measured in inches ( $a_0 \leq r \leq a$ ).



- $w_p$  = DEFLECTION OF THE PANEL MEASURED IN INCHES IN THE REGION  $a_0 \leq r \leq a$
- $n$  = MEMBRANE FORCE PER UNIT WIDTH OF PLATING MEASURED IN POUNDS PER INCH
- $a$  = RADIUS OF A CIRCULAR PANEL MEASURED IN INCHES
- $w_{a_0}$  = DEFLECTION AT THE EDGE OF THE LOADED ZONE
- $p$  = UNIFORM LOAD MEASURED IN POUNDS PER SQUARE INCH IN A SMALL CIRCLE OF RADIUS  $a_0$  HAVING ITS ORIGIN AT THE CENTER OF THE PANEL
- $t$  = PLATE THICKNESS

Figure 20 – Statically Loaded Circular Panel with Fixed Boundary

Figure 20 shows the panel boundaries as fixed boundaries. The assumption of fixity in bending and tension is made for all the theoretical derivations although complete fixity is unlikely in either the underbody of the full-scale craft or in the experimental facility. Some degree of fixity does exist, however, and therefore the approximation of fixity more accurately models the damage mechanism than would an assumption of no fixity. Under

conditions of partial fixity of the panel boundaries, less energy would probably be absorbed by the impacted panel than predicted here, but additional energy would be absorbed in adjacent structure. Deflection to rupture would also increase somewhat under conditions of partial fixity.

The following equations can be obtained from the equilibrium of forces in the Z-direction for  $a_0 \leq r \leq a$

$$\begin{aligned}
 p \pi a_0^2 - (2\pi r)n \left( - \frac{dw_p}{dr} \right) &= 0 \\
 p \pi a_0^2 + 2\pi r n \frac{dw_p}{dr} &= 0 \\
 2r n \frac{dw_p}{dr} + p a_0^2 &= 0
 \end{aligned} \tag{1}$$

Integrating Equation (1) yields:

$$\begin{aligned}
 \int_w^0 dw_p &= \int_r^a - \frac{p a_0^2}{2r n} dr \\
 -W_p &= - \frac{p a_0^2}{2n} \ell_n r \Big|_r^a \\
 W_p &= \frac{p a_0^2}{2n} [\ell_n a - \ell_n r] \\
 W_p &= \frac{p a_0^2}{2n} \ell_n \frac{a}{r}
 \end{aligned} \tag{2}$$

The deflection of the panel at the edge of the loaded area  $W_{a_0}$  may be defined by substituting  $r = a_0$  in Equation (2). This location is the point where the impact obstacle is no longer tangent to the deflected panel.

Since the total deflection at the center of the panel includes both the membrane deflection at  $a_0$  and the protrusion deflection  $\delta$ , the two components of the total deflection at the center of the panel are added to define the panel deflection in Equation (3):

$$W = \delta + \frac{P}{2n\pi} \ell_n \frac{a}{a_0} \tag{3}$$

where  $P = p \pi a_0^2$

$\delta$  = local protrusion or deflection resulting from plate conformation with the obstacle shape (Figure 21)

$W$  = total deflection of center of circular panel including protrusion deflection

The protrusion deflection  $\delta$  is that deflection which results primarily from local bending as the portion of the panel in contact with the impact obstacle conforms to the shape of the obstacle. Appendix A presents the derivation and definition of the protrusion deflection.

The membrane force per unit width of plate is defined by

$$n = \sigma_a t$$

where  $n$  is the membrane force per unit width of plate and  $\sigma_a$  is the axial or membrane stress.

Since most of the load-deflection curve for unstiffened panels is in the plastic membrane region where the membrane stress is equal to the yield stress, it is reasonable to approximate  $\sigma_a$  as the yield stress.

The load-deflection equation may then be written as:

$$P = \frac{2\pi \sigma_y t (W-\delta)}{\ln a/a_0} \quad (4)$$

Equation (4) may be solved if the value of  $a_0$  is known. A reasonable estimate for  $a_0$  is easily obtained from the obstacle geometry and, therefore, Equation (4) is the theoretical load-deflection relationship. An accurate value for  $a_0$  is not necessary for significant membrane response since the term is secondary. Figure 21 shows the dimension  $a_0$  on the deflected panel geometry. Figure 22 illustrates the good correlations achieved by using this method for large deflections. The Japanese<sup>3</sup> have also used a similar method with equally good correlation in ship collision research on nuclear-powered ships.

The theoretical analysis is static since the collision response of the panel is dictated not by a load pulse on a structure but by a deflection of the structure imposed by the craft moving toward the obstacle. The mass of the panel is small relative to the mass of the craft

---

<sup>3</sup>Harima, T. et al., "Research on the Collision-Resisting Construction of the Sides of a Nuclear-Powered Ship," Mitsubishi Heavy Industries Technical Review, No. 2, p. 147 (1962).

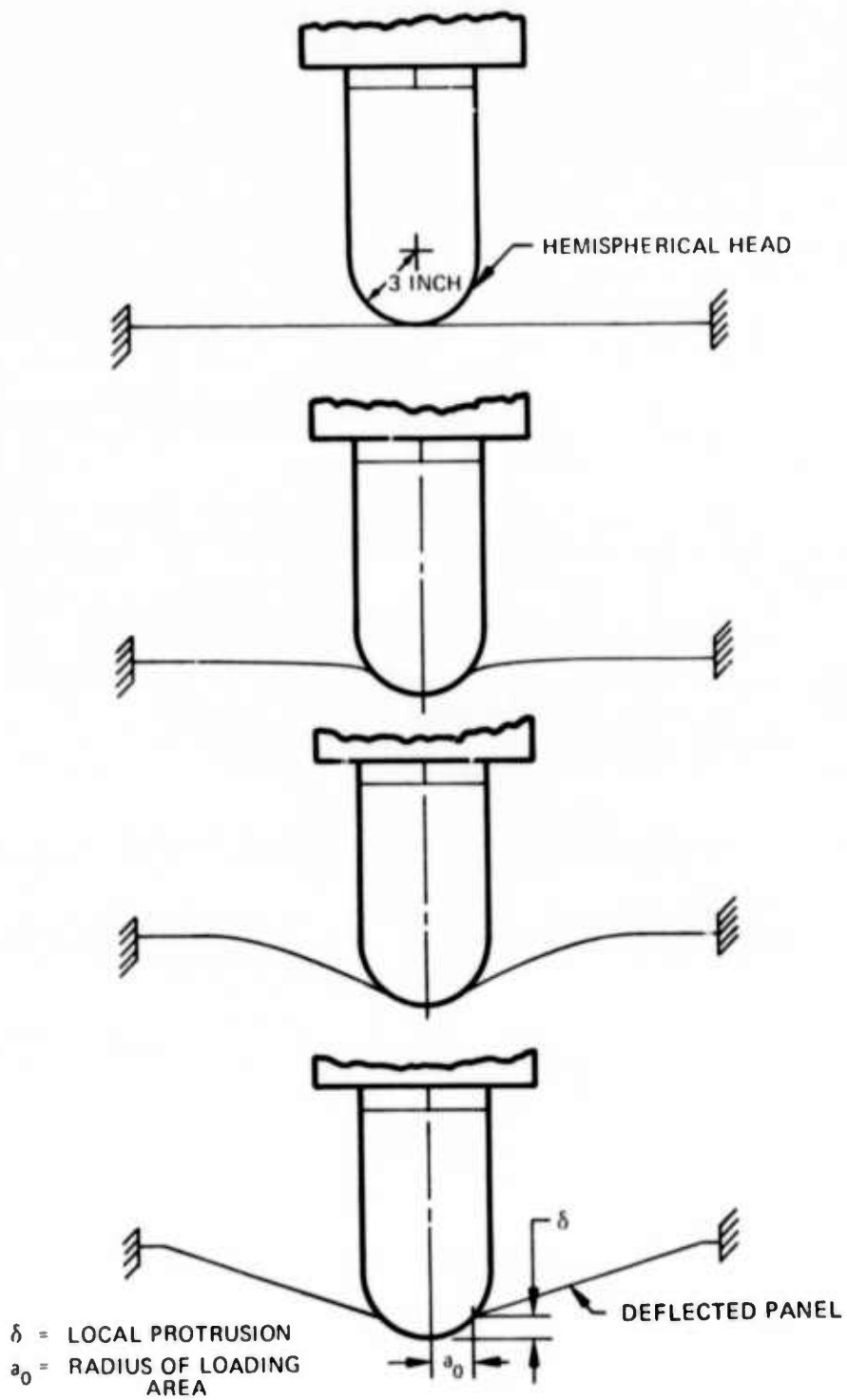


Figure 21 - Local Protrusion and Radius of Loading Area for Unstiffened Panel

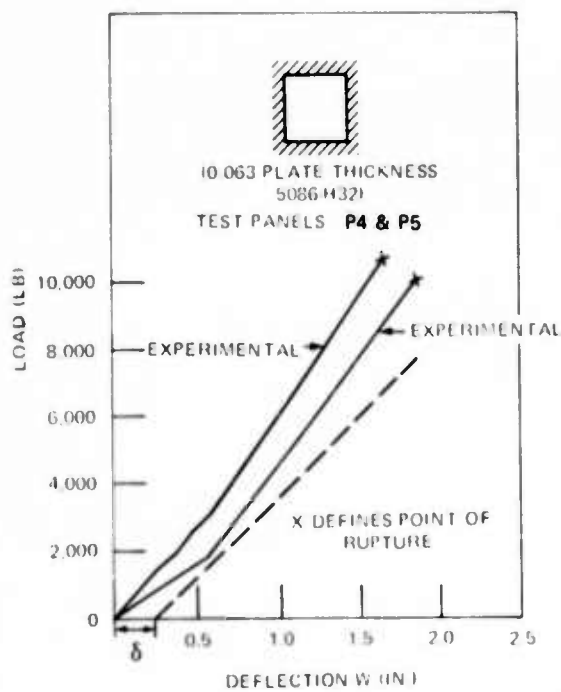
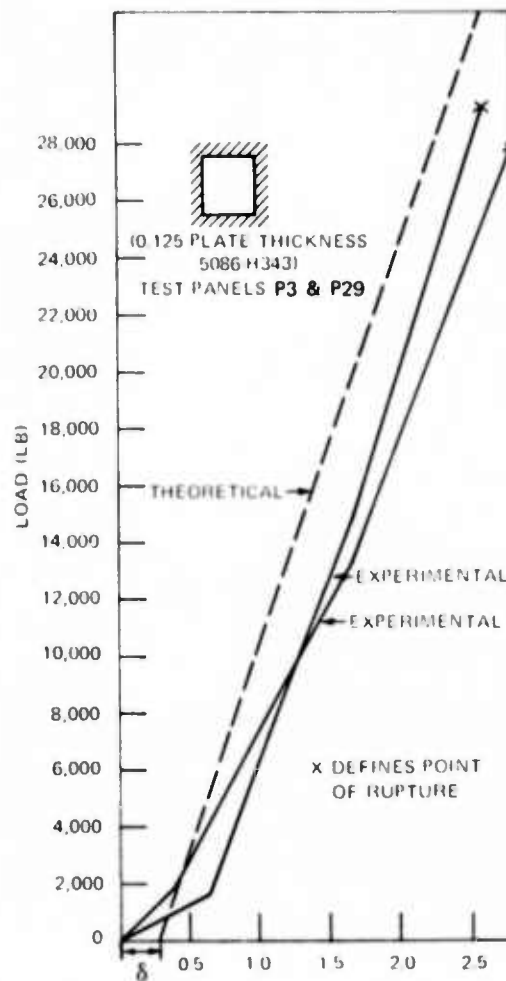
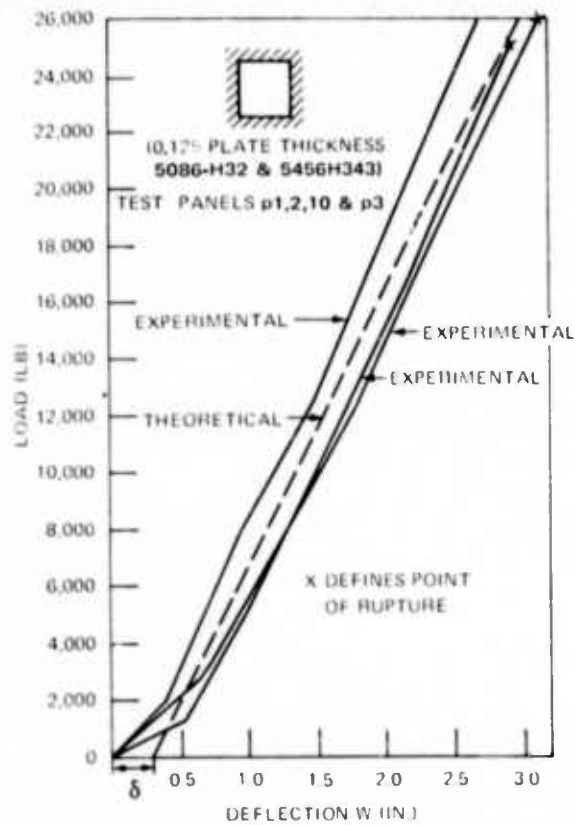


Figure 22 – Theoretical versus Experimental Load-Deflection Curves for Aluminum Unstiffened Panels

and the obstacle is assumed to be rigid and unmoving. Since the imposed deflection is defined through the velocity and mass of the entire craft, the problem is viewed as one of static energy absorption and the inertial forces in the plate are neglected.

### STIFFENED SQUARE PLATES

Stiffened panels (1 X 1) have been shown to display both bending- and membrane-type behavior, depending on the panel geometry. These panels may be analyzed by assuming a lattice structure of fixed-end beams (stiffeners) with an effective width of plating<sup>4</sup> (Figure 23) defined as follows:

$$b_e = 2t \sqrt{\frac{E}{\sigma_y}}$$

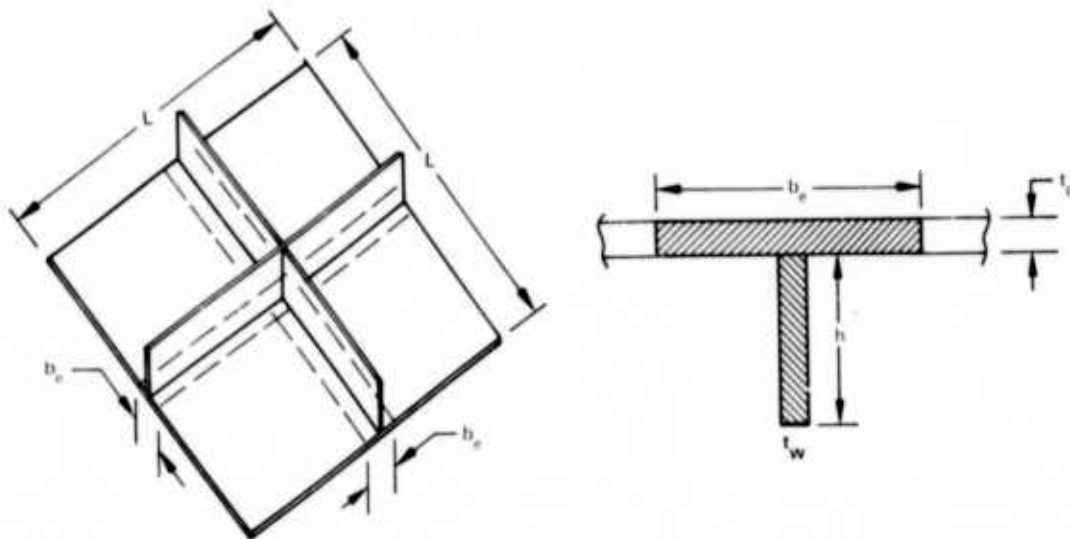


Figure 23 - Effective Width of a (1 X 1) Web-Stiffened Panel

<sup>4</sup>NAVSEC Design Data Sheets DDS 1100-3 (7 Mar 1956).

where  $b_e$  = effective width of plating

$t$  = plate thickness

$E$  = Young's modulus

$\sigma_y$  = yield stress

The equation used for effective width of plating enables an approximation of the amount of plate material which acts with the stiffener in bending. For purposes of this study, the approximation is applied uniformly to cross sections at center span and at the boundaries of the panel. Actually, a different approximation could be used for cases where the plate is in tension and in compression. Similarly, different approximations could be used for elastic and plastic conditions. These refinements are not considered necessary, however, for our purposes.

The lattice structure is deformed progressively until plastic hinges form at the center of the panel and at the boundaries. Further deformation increases the membrane stresses in the lattice structure until the panel fails.

One way to view the effect of membrane (axial) stress is to consider that the axially stressed zone of material which develops is sufficiently large to carry the membrane force. The zone is centered about the combined stress neutral axis and, therefore, the membrane load does not contribute to the plastic moment. The plastic moment is reduced, however, by the change in the stress profile. The neutral axis for combined stress shifts in one direction or the other from the location for pure bending, depending on the sign of the bending moment (Figure 24). The effect of membrane loading on the plastic bending resistance for a T-section (i.e., a plate stiffened with a rectangular web) is similar for a flanged stiffener, but the calculation becomes more complicated because of the number of different cases which may occur with reference to location of the membrane stress zone.

#### LOAD-DEFLECTION RELATIONSHIP FOR STIFFENED PANELS

It is possible to define the load-deflection relationship for a stiffened panel if the membrane stress, the protrusion deflection, and the reduced plastic moment are known.

The protrusion deflection, i.e., that portion of the total panel deflection caused by local conformation of the panel to the obstacle shape, is approximated for a hemispherically shaped obstacle as follows (see Appendix A)

$$\delta = R \left[ 1 - \cos \left( \tan^{-1} \left( \frac{2W}{L} \right) \right) \right] \quad (5)$$

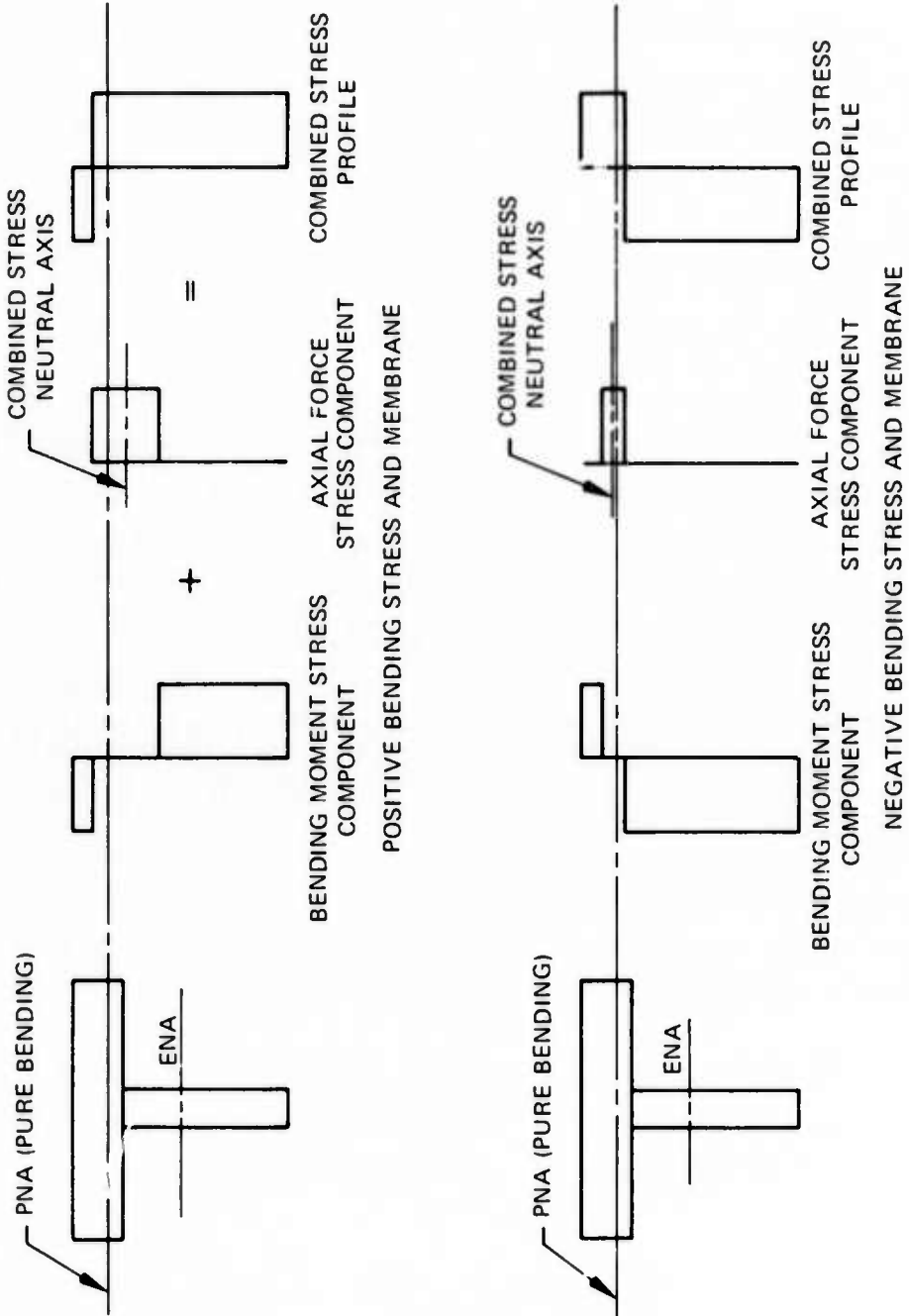


Figure 24 – Stress Profile Assuming Combined Bending and Membrane Response

where  $\delta$  = protrusion deflection in inches

$R$  = radius (in inches) of the hemisphere which defines the shape

$W$  = total deflection (in inches) of the center of the panel

$L$  = the span length (in inches) of the stiffeners

In order to calculate the effect of the membrane stress on the ability of the section to carry plastic moment, the membrane stress must first be defined as a function of total deflection. Equation (6), derived in Appendix B, defines the membrane stress as a function of total deflection and protrusion deflection:

$$\sigma_s = E \left( \frac{W}{L} \right)^2 \left[ 2 - \frac{4\delta}{W} + \frac{2\delta^2}{W^2} \right] \quad (6)$$

where  $\sigma_s$  is membrane stress and  $E$  is Young's modulus, both in pounds per square inch.

The stiffened panel structure may be approximated by a set of beams composed of the stiffeners and an effective width of plating. The load corresponding to the deflection ( $W$ ) of that set of beams may be computed from the free-body diagram of the deflected panel shown in Appendix B provided the reduced plastic moments for the center of the span and the ends of the span ( $M_c$  and  $M_e$ , respectively) are known. The reduced plastic moments may be computed by using the membrane stress calculated in Equation (6).

The reduced plastic moments  $M_c$  and  $M_e$  were calculated by using a computer program written specifically for that purpose. The approach was to assume a location for the combined stress neutral axis. This implies a plastic moment since the axially stressed region of the cross section must be located such that no moment about the neutral axis results from the axial stress. If the regions stressed axially and in bending are known, then the plastic moment and the membrane force may be determined. The membrane force is then compared to the membrane force calculated for the panel deflection using Equation (6) and the cross-sectional area  $A$ . If the two membrane forces agree, then the assumed combined stress neutral axis was correct and the reduced plastic moment is the plastic moment of the solution. If not, the location of the combined stress neutral axis is shifted and a new solution calculated until the iteration produces a satisfactory comparison.

$$P = \frac{4N}{L} [M_c + M_e] + \frac{4N}{L} [\sigma_s A W] \quad (7)$$

where  $P$  = total load (in pounds) concentrated at the center of the panel required to cause deflection  $W$

A = cross-sectional area of the stiffener and effective plate width

N = number of stiffeners passing through the collision point; [N = 1, (1 × 0) or  
N = 2 (1 × 1)]

The load-deflection curve is therefore computed by selecting a set of deflections and using Equations (5)–(7) to predict the companion set of loads.

Each beam behaves elastically until plastic deformation occurs and plastic hinges form at center span and at the ends of the beams. If the collision force is assumed to be a concentrated load at the center of the span, then plastic hinges form simultaneously at the ends and middle of the beam for this particular statically indeterminate structure. The plastic moment is the maximum bending moment that a section can resist. Ideally, all the material of the beam section is stressed to the yield stress. The value of the plastic moment remains constant until the beam must carry an axial or membrane loading. As previously mentioned, if a membrane stress is present, the plastic moment is reduced.

Forms of Equations (6) and (7) were used by Harima et al.<sup>3</sup> in their theoretical load-deflection definition for mild and high strength steel panels. The equations were found to yield good correlation with experimental results.

## COMPARISON OF THEORETICAL AND EXPERIMENTAL RESULTS

Figures 22 and 25–32 compare the experimental and theoretical load-deflection curves. Each figure includes a description of the type of panel and the panel geometry. Experimental results from several tests on the same panel geometry are included where available. Note that provided deflection at rupture is known, the theoretical method presented here gives good correlation with experimental load-deflection curves for both unstiffened and web stiffened panels.

The theoretical load-deflection curve in Figure 26 shows a depression following a fairly constant load. Apparently the membrane stresses reduced the capability of the panel section to carry a plastic bending moment and yet the increase was insufficient to take up the slack in the total load-carrying capability. This effect is most pronounced in deep panels where the flexural deflections are small and the membrane forces in the early phases of plastic membrane behavior act at very shallow angles to the horizontal.

This theoretical depression in the load-deflection curve may be due to the simplifying approximations of the theoretical method. It seems logical that a real panel would maintain its load-carrying capability through expansion of the plastic hinges and then through shear and bending deformation of the remainder of the panel. Some panels did show experimental evidence of the depression; however, this may or may not have been a result of the theoretically described phenomenon.

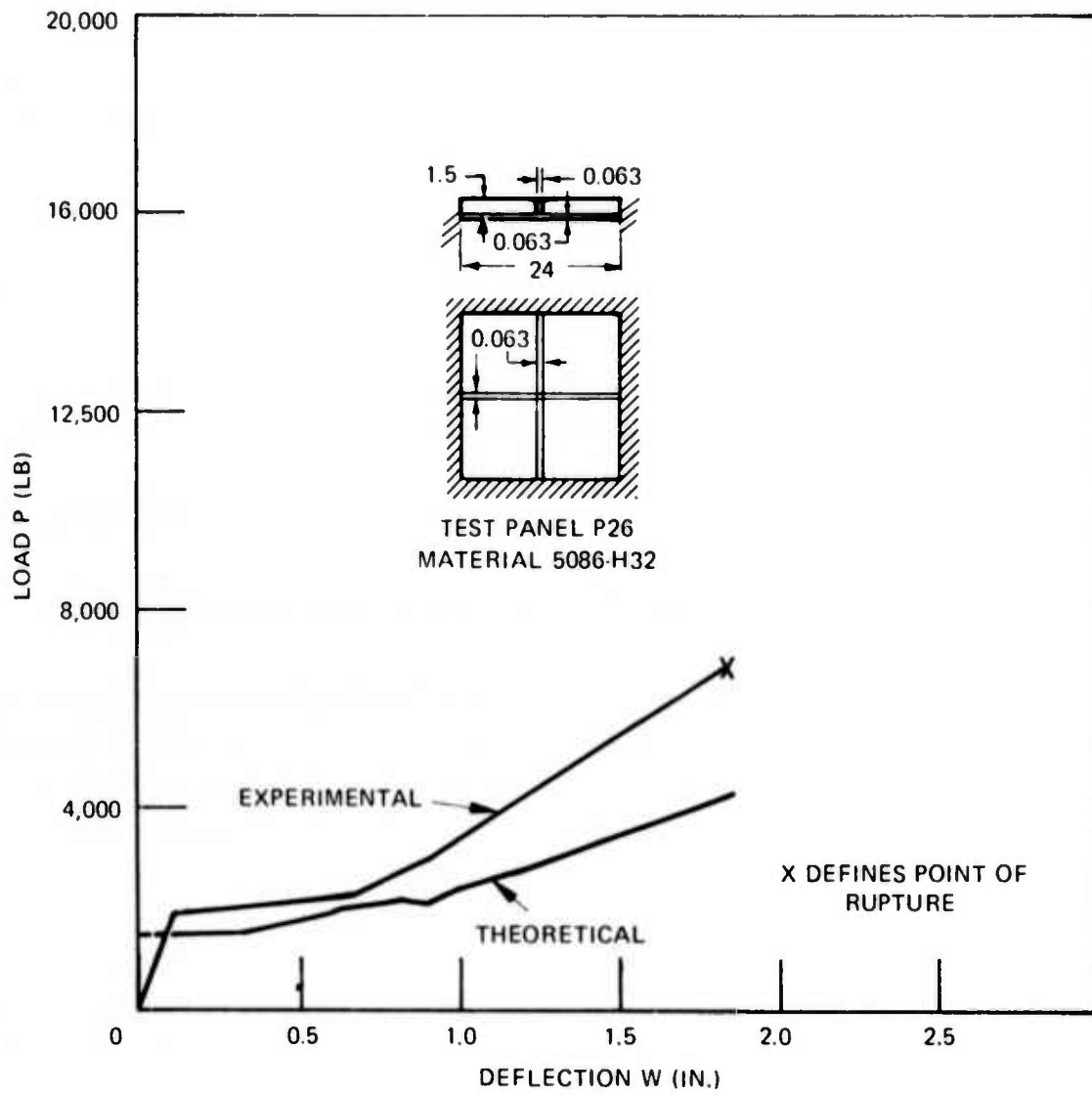


Figure 25 – Theoretical versus Experimental Load-Deflection Curves for Aluminum Web-Stiffened Panel-Type I

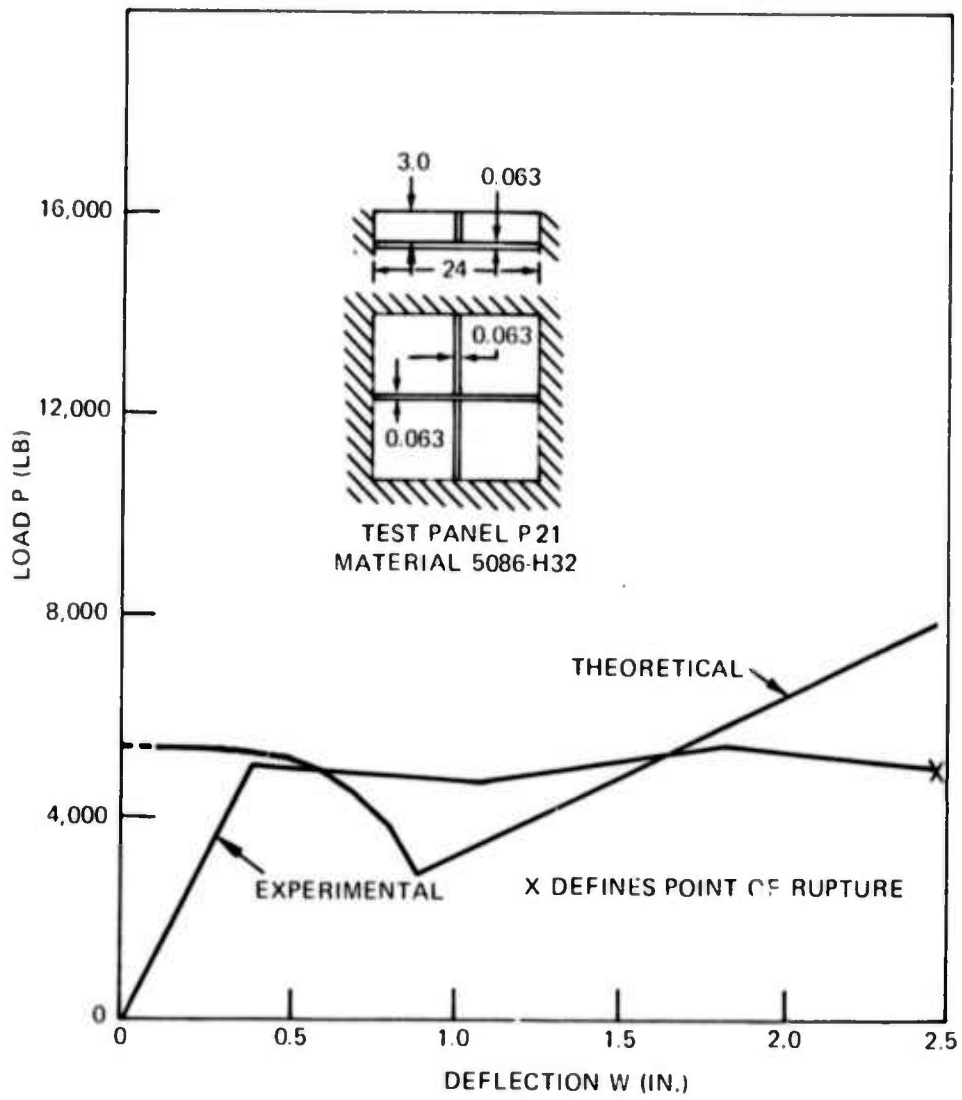


Figure 26 - Theoretical versus Experimental Load-Deflection Curves for Aluminum Web-Stiffened Panel-Type II

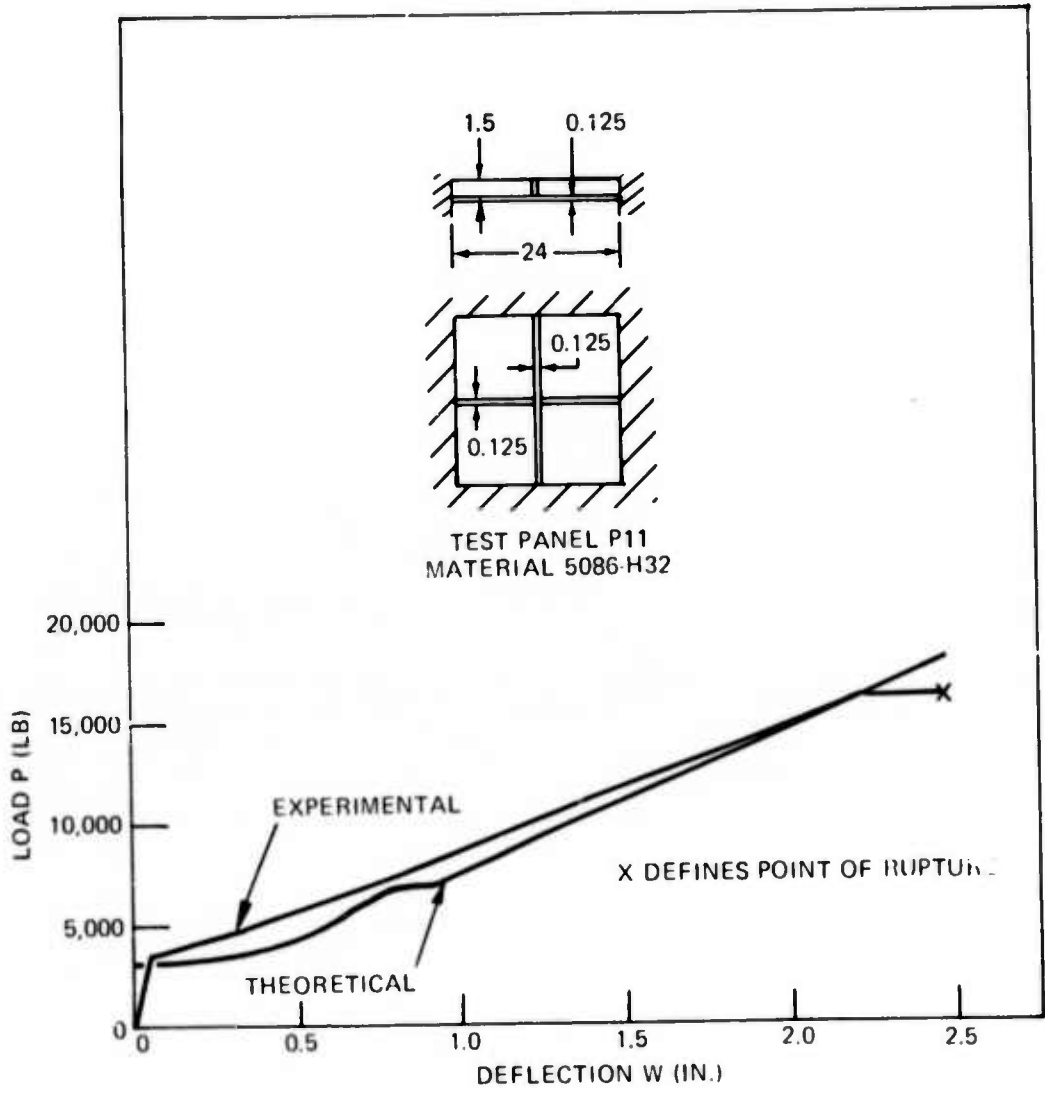


Figure 27 – Theoretical versus Experimental Load-Deflection Curves for Aluminum Web-Stiffened Panel-Type III

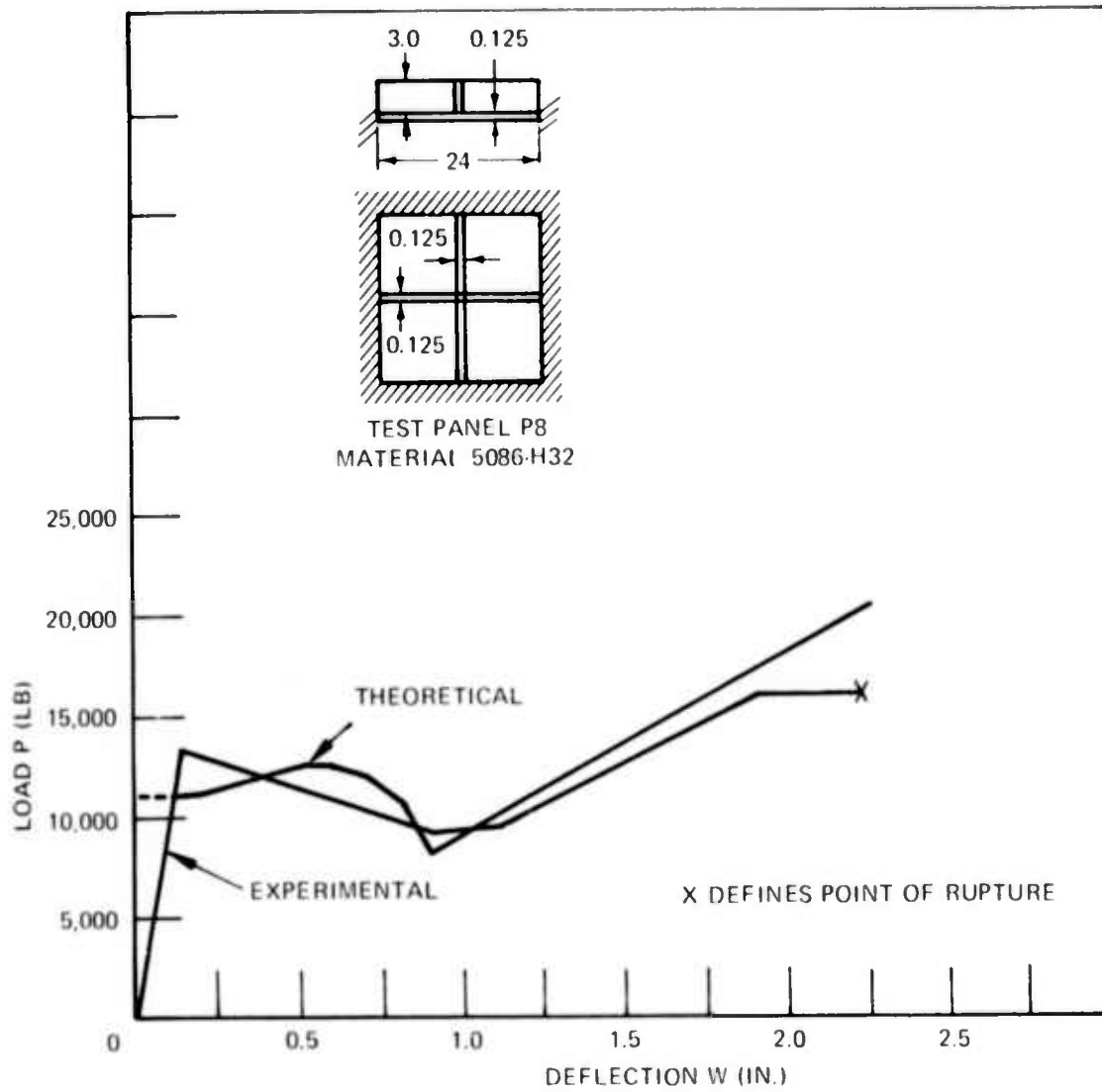


Figure 28 - Theoretical versus Experimental Load-Deflection Curves for Aluminum Web-Stiffened Panel-Type IV

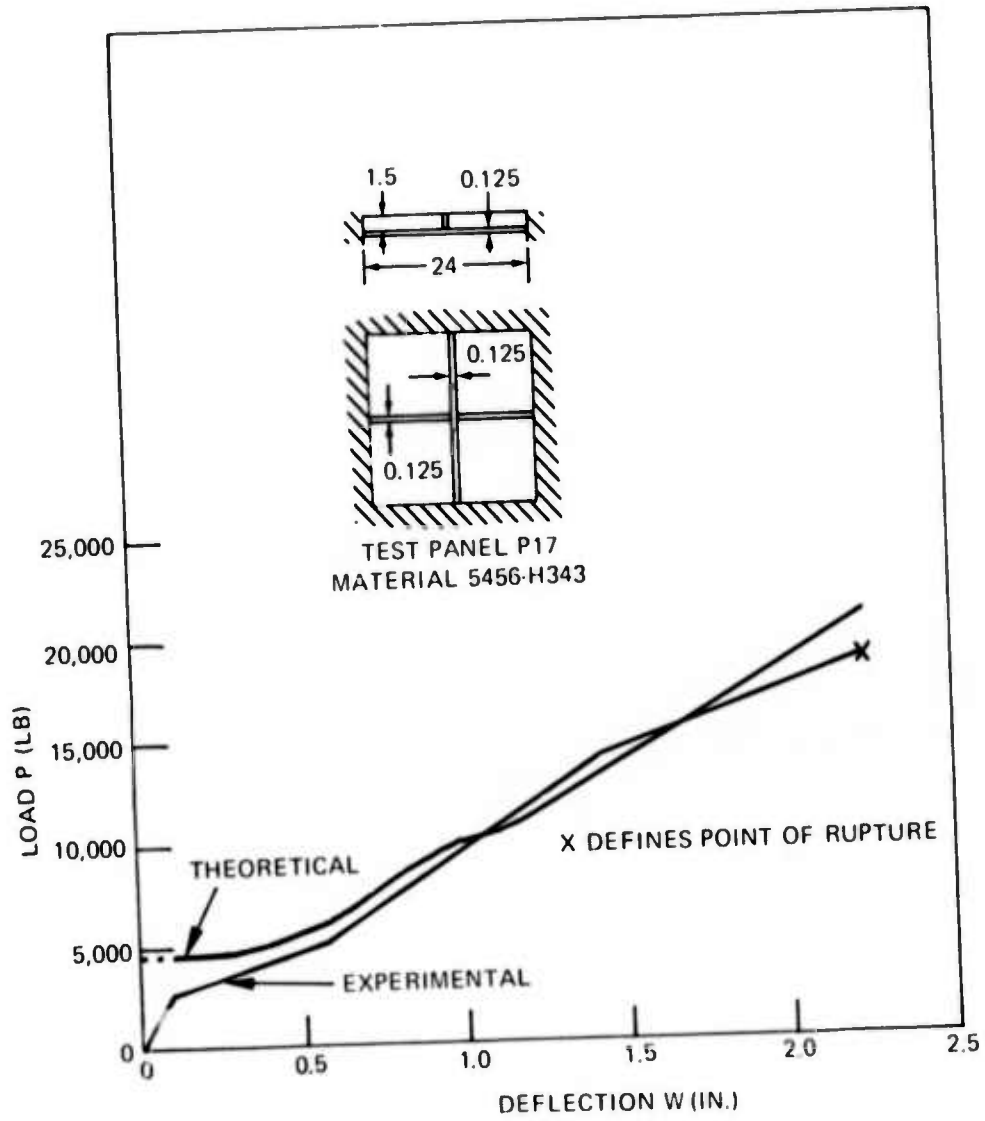


Figure 29 - Theoretical versus Experimental Load-Deflection Curves for Aluminum Web-Stiffened Panel-Type V

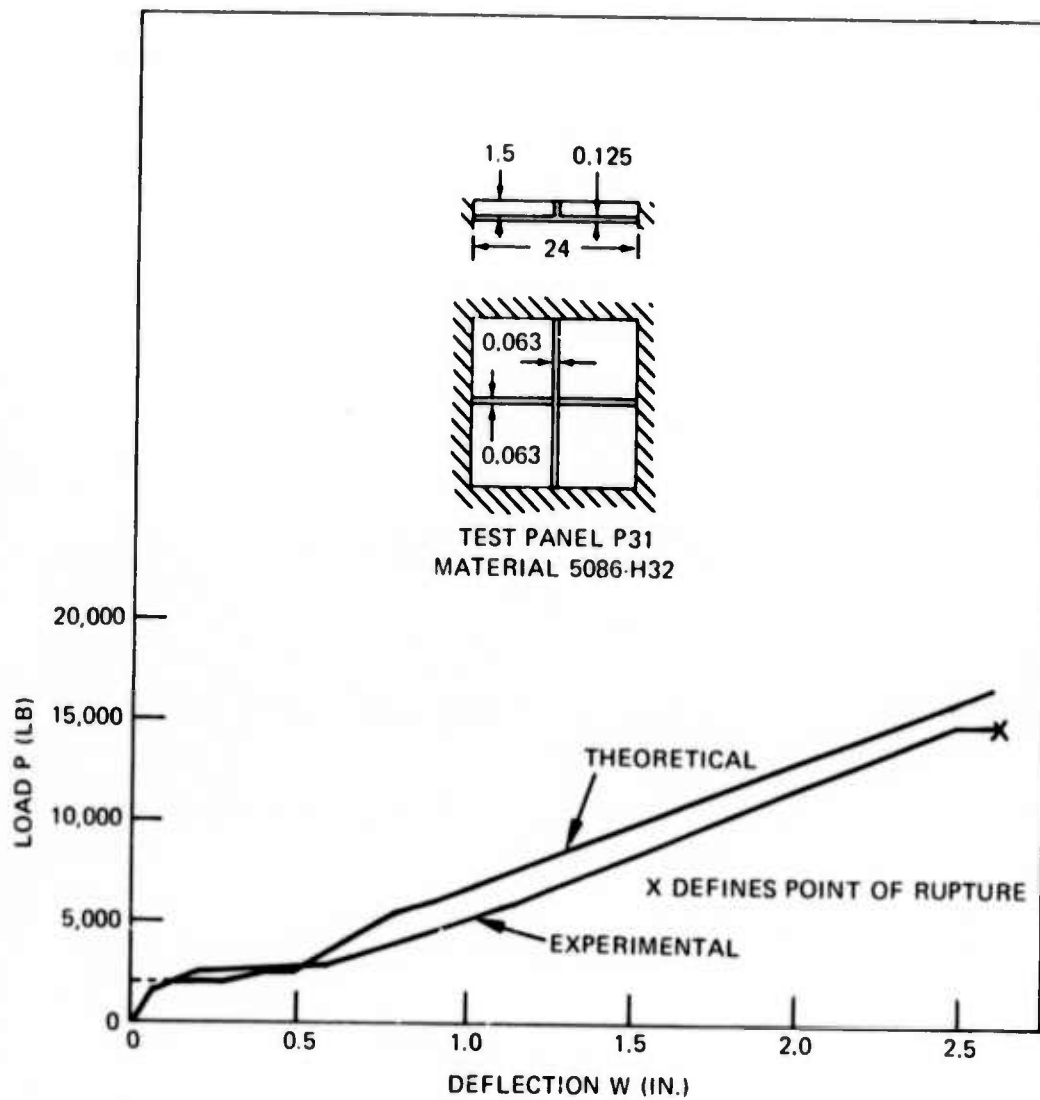


Figure 30 – Theoretical versus Experimental Load-Deflection Curves for Aluminum Web-Stiffened Panel-Type VI

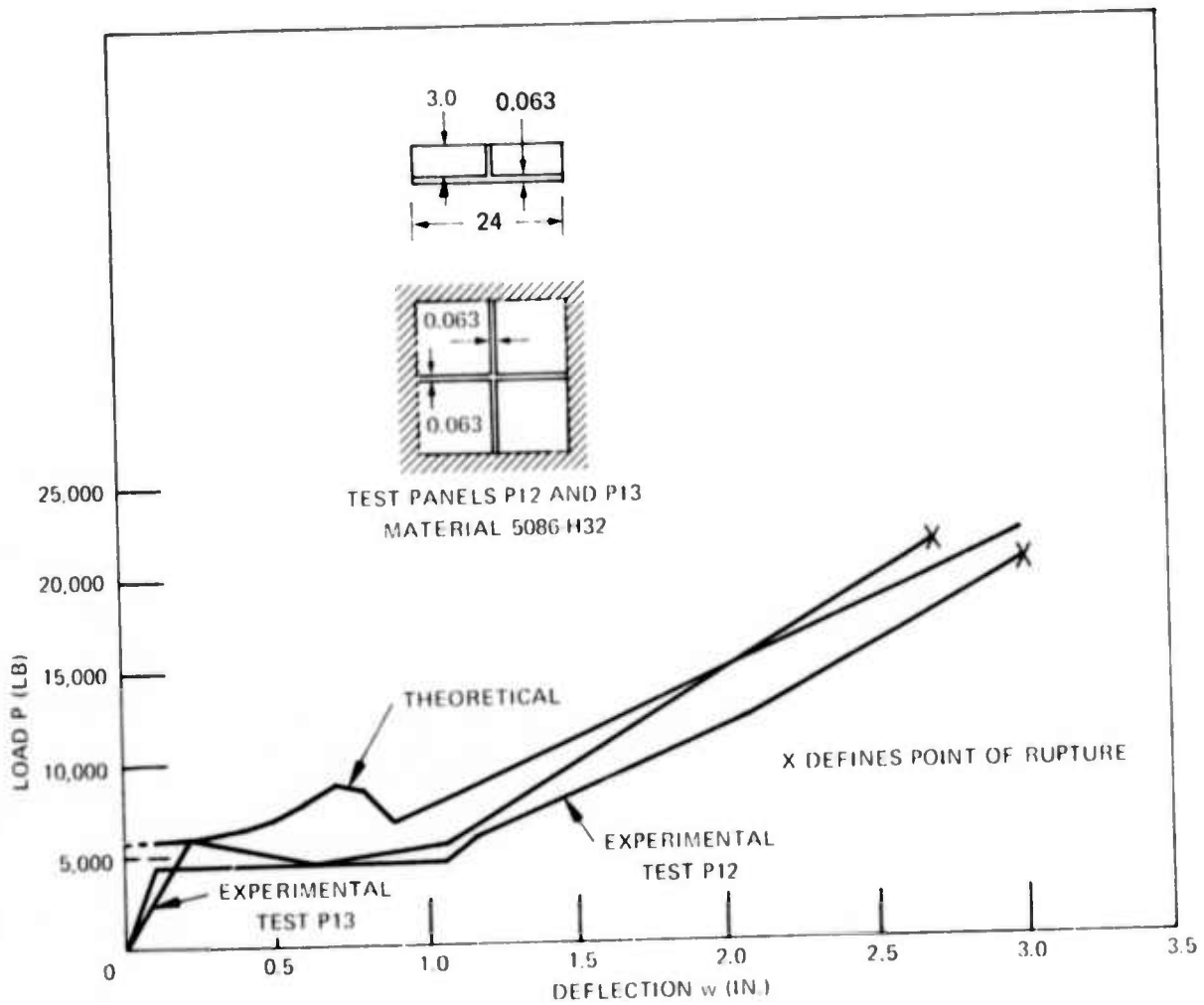


Figure 31 – Theoretical versus Experimental Load-Deflection Curves for Aluminum Web-Stiffened Panel-Type VII

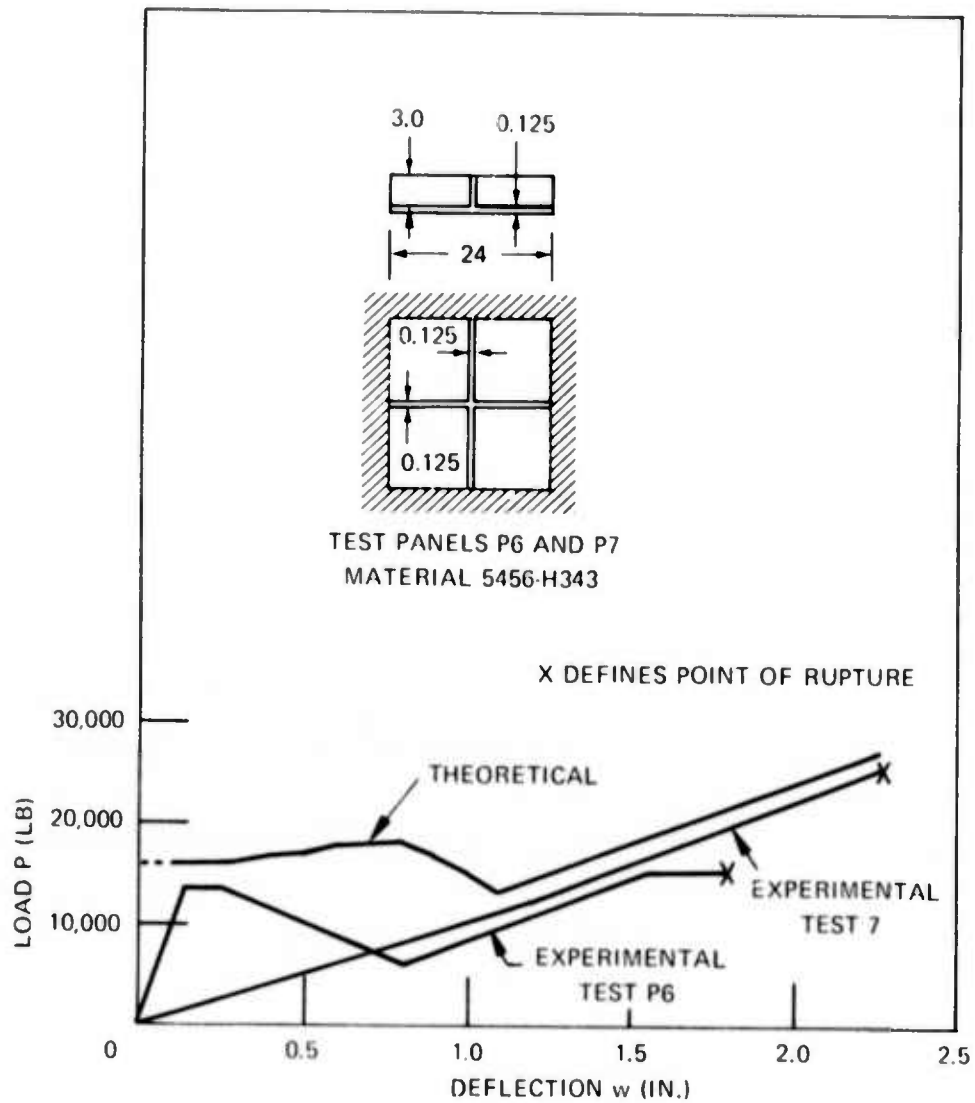


Figure 32 – Theoretical versus Experimental Load-Deflection Curves for Aluminum Web-Stiffened Panel-Type VIII

Note also that the elastic response of the panel was not calculated. Instead, plastic bending was assumed to begin immediately on deflection of the panel. This approximation is reasonable inasmuch as most of the energy is absorbed in plastic response of the panel.

Since a successful theoretical method for determining the deflection at rupture has not been developed to date, it is not possible to give a completely theoretical determination of the energy-absorbing capability of a panel. However, if the experimental deflections at rupture are used with the theoretical load-deflection curves, it is possible to compare the experimental energy-absorbing capability with the energy theoretically absorbed to the point of rupture.

Comparisons of the energy absorbed for both the experimental and theoretical results indicate good correlation. The theoretical energy absorption was within 17 percent of the values obtained experimentally.

One test panel failed prematurely during the first inch of deflection probably due to a defective weld. Since the theoretical load-deflection curve assumes a perfect panel, correlation of both the load-deflection curve and the energy-absorbing capability was not as good for this panel as for the others.

The theoretical energy-absorbing capability for the (1 X 1) web-stiffened panels was determined as described previously by integrating the theoretical load-deflection curves to the experimental rupture deflection. The average value of deflection to rupture for the (1 X 1) web-stiffened panels was 2.44 in.

A range of deflections to rupture for unstiffened panels of 2.87, 2.71, and 1.77 in. were observed for 0.125-in. 5086-H32, 0.125-in. 5456-H343, and 0.063-in. 5086-H32 panels, respectively.

Krappinger<sup>5</sup> has developed a semiempirical relationship based on the experimental results of mild and high strength steel plates under loading conditions similar to those investigated here. However, the method contains too many experimentally defined constants to be confidently extended to different plate materials and different geometries without further experimental verification.

It is recommended that the approach used at NSRDC\* for defining the deflection to rupture of stiffened and unstiffened steel panels be pursued to define the deflection at rupture of the aluminum ASEV underbody panel.

---

<sup>5</sup>Krappinger, O., "Collision Protection of Nuclear Ships," University of Michigan, ORA Project 07990, under contract with the Maritime Administration, U.S. Department of Commerce Contract MA-2564, Task 9 (May 1966).

\*Reported informally by S. Ziliacus et al. in NSRDC Technical Note SD 174-433 of 11 February 1974.

## APPLICATIONS OF THE ENERGY-ABSORBING UNDERBODY PANEL FOR ASEV'S

As previously mentioned, some measure of protection must be provided to sustain a craft against possible underbody collision during operations in the Arctic environment. Figure 33 shows the damaged underbody of an SK-5 following vertical impact with an ice obstacle during the 1971 SEV Arctic trials.

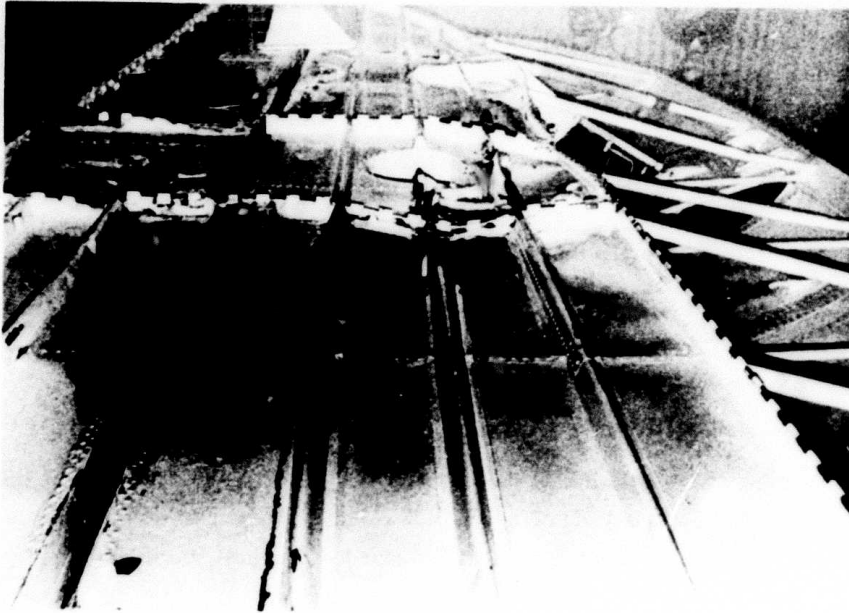


Figure 33 – Underbody of SK-5 following Impact on an Ice Obstacle during 1971 SEV Arctic Trials

The underbody must be capable of absorbing the vertical kinetic energy of the ASEV within limited deflections. Equation (8) relates the vertical kinetic energy  $E_C$  to the mass of the craft  $M$  and the vertical impact velocity  $V_i$ . The vertical impact velocity  $V_i$  is taken as the vertical velocity component toward the obstacle as shown in Figure 2.

$$E_C = \frac{1}{2} (M) (V_i)^2 \quad (8)$$

Because ice obstacles are brittle<sup>6</sup> and can be expected to absorb very little energy, the kinetic energy must be entirely dissipated by the underbody panels in order to avoid damage. Figure 34 indicates the vertical kinetic energy that a craft must absorb as a function of the allowable vertical impact velocity for several craft weights.

Based on the test results and the scaling laws derived, an estimate may be made of the weight penalty associated with protecting different sizes of ASEV's against underbottom collision at various impact velocities. ASEV craft weights of 150 and 540 tons are investigated at impact velocities of 3 and 5 ft/sec. The program goal is to design the underbody structure to resist collisions at vertical impact velocities of 3 to 5 ft/sec at a weight penalty no greater than 10 percent of the craft weight.

An energy scaling law was developed to extrapolate the energy-absorbing capabilities of the experimental model a given test panel configuration to a full-size prototype configuration. A dimensional analysis was conducted for the underbody collision phenomena, including structural response terms, and the following scaling law was derived. If the prototype panel is fabricated of the same material and has the same degree of imperfection, then

$$E_p = \lambda^3 E_m$$

where  $E_p$  = energy of the prototype energy protection system

$E_m$  = energy of the model test panel

$\lambda$  = geometric scale factor

The dimensional analysis is shown in Appendix D.

The model chosen was the aluminum (5086-H32) (1 X 1) panel with flanged stiffeners. This particular test panel was selected because it displayed the highest specific energy absorption (energy absorbed at rupture per pound of material) of all the (1 X 1) panel geometries tested. A stiffened rather than an unstiffened panel was chosen because it represents a more realistic structure for ASEV use in terms of panel stability. Its dimensions are as follows:

Panel length  $L = 24$  in.

Plating thickness  $t_p = 0.125$  in.

Web stiffener thickness  $t_w = 0.125$  in.

Web stiffener height  $h = 3.0$  in.

Flange thickness  $t_f = 0.125$  in.

Flange width  $w_f = 2.0$  in.

---

<sup>6</sup>Pounder, E.R., "Physics of Sea Ice," Pergamon Press, New York (1965).

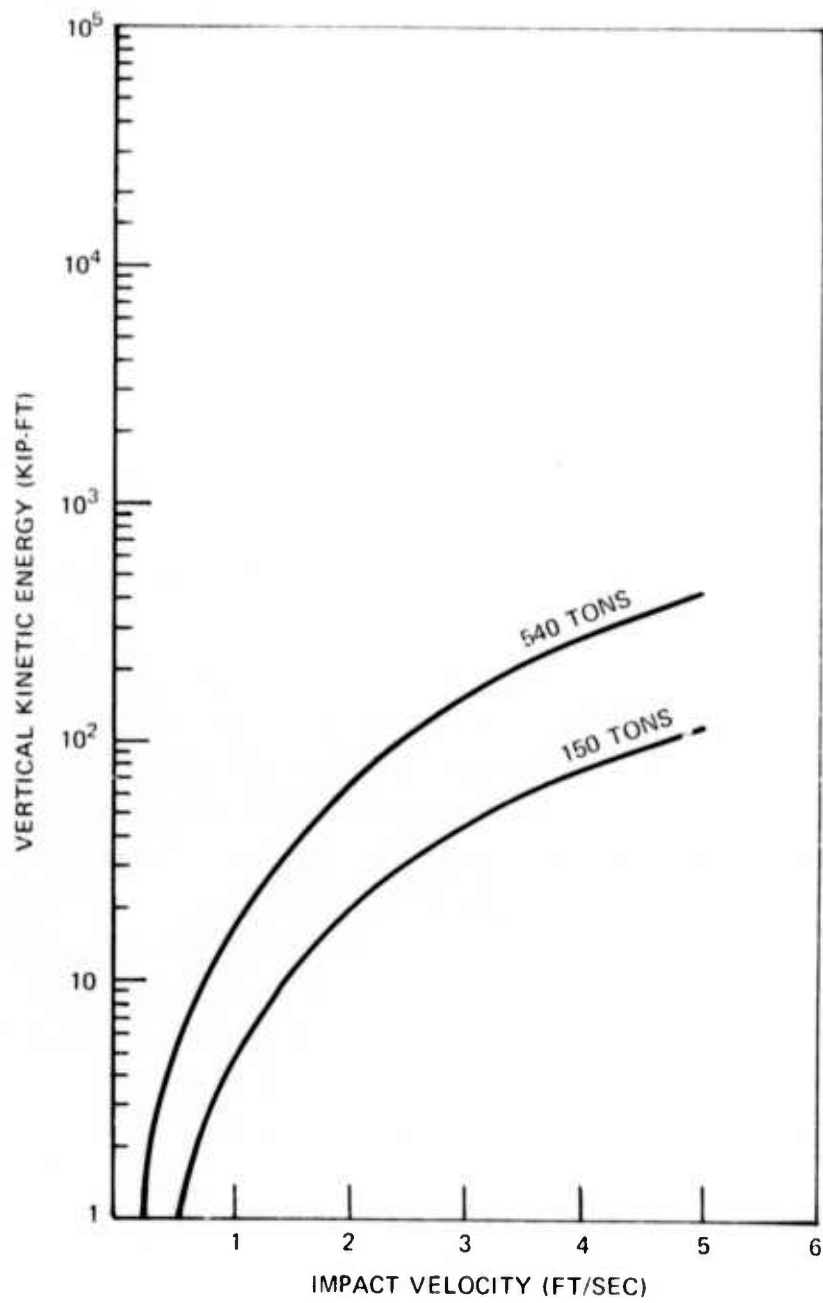


Figure 34 – Vertical Kinetic Energy of 150- and 540-Ton ASEV's as a Function of Impact Velocity

(It should be noted that one test panel exhibited a higher specific energy absorption than the panel utilized for full-scale ASEV underbody definition. A 3 x 0 flanged-stiffened panel absorbed about 116 percent more energy for the same weight of panel. This panel was not selected for ASEV underbody definition since only one test was conducted for this geometry. The geometry does show promise, however, and it is recommended that further work be done in the area of panels stiffened in this manner.)

The relative scale of the prototype underbody protection system may be determined by using Equation (9), solving for  $\lambda$ , and scaling up the dimensions of the test panel. Here  $E_m$  is the maximum energy-absorbing capability of a test panel.

$$\lambda = \left[ \frac{M V_i^2}{2} / (E_m) \right]^{1/3} \quad (9)$$

Equation (9) is plotted in Figure 35 as a function of energy-absorbing requirement. It is assumed for purposes of this study that the obstacle impacts only one panel and that the vertical kinetic energy ( $M V_i^2/2$ ) of the craft must be absorbed within the single panel. It is also assumed that the impact occurs at the center of the panel and on the craft center of gravity so that no energy is absorbed by craft rotation. Since  $\lambda$  is a geometric scale factor, the weight scales as  $W_p = \lambda^3 W_m$ . Here  $W_p$  and  $W_m$  are respectively the panel weight of the prototype system and that of the model system or test panel.

The weight of the total underbody protection system is calculated by multiplying the prototype panel weight by the total number of panels necessary to protect the entire underbottom. Thus the weight penalty for underbody collision protection is simple to determine. The weight for the total underbody protection system is plotted for various impact velocities in Figure 36 for two ASEV's of different size. If the weight for the underbody structure is limited to 10 percent of the craft weight, the 150- and the 540-ton craft are respectively capable of absorbing the energy of a 4.35- and a 5.70-ft/sec collision.

The impact velocity calculated here is based on the energy absorption to rupture. If a factor of safety of 1.5 on the energy-absorbing capability is used, the modified version of Equation (9) including the factor of safety is as shown in Equation (10). Note that if a factor of safety of 1.5 is used on the energy, the weight is also increased by 50 percent.

$$\lambda = \left[ \frac{E_c (1.5)}{E_{exp}} \right]^{1/3} \quad (10)$$

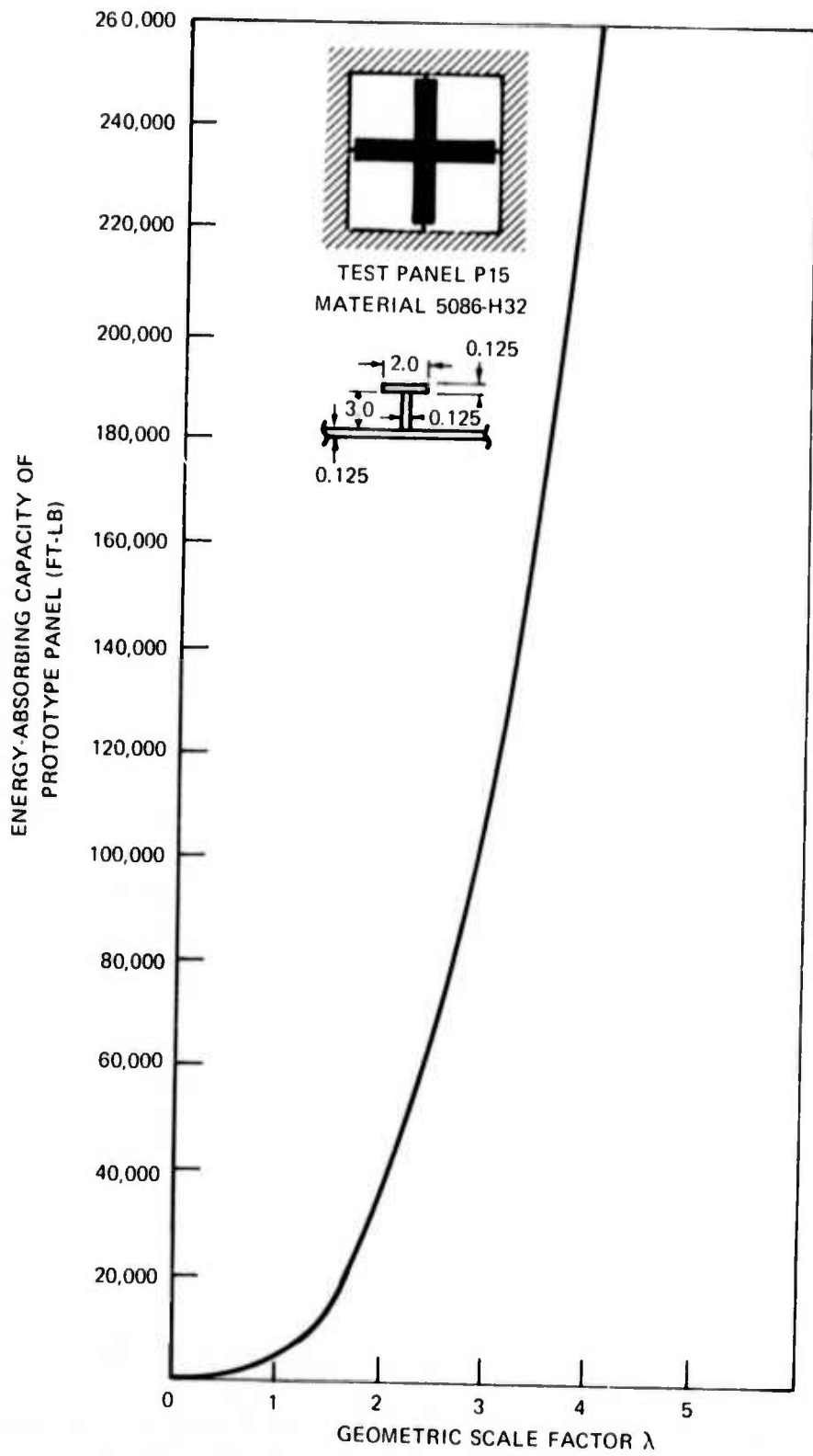


Figure 35 -- Energy-Absorbing Capacity versus Scale Factor

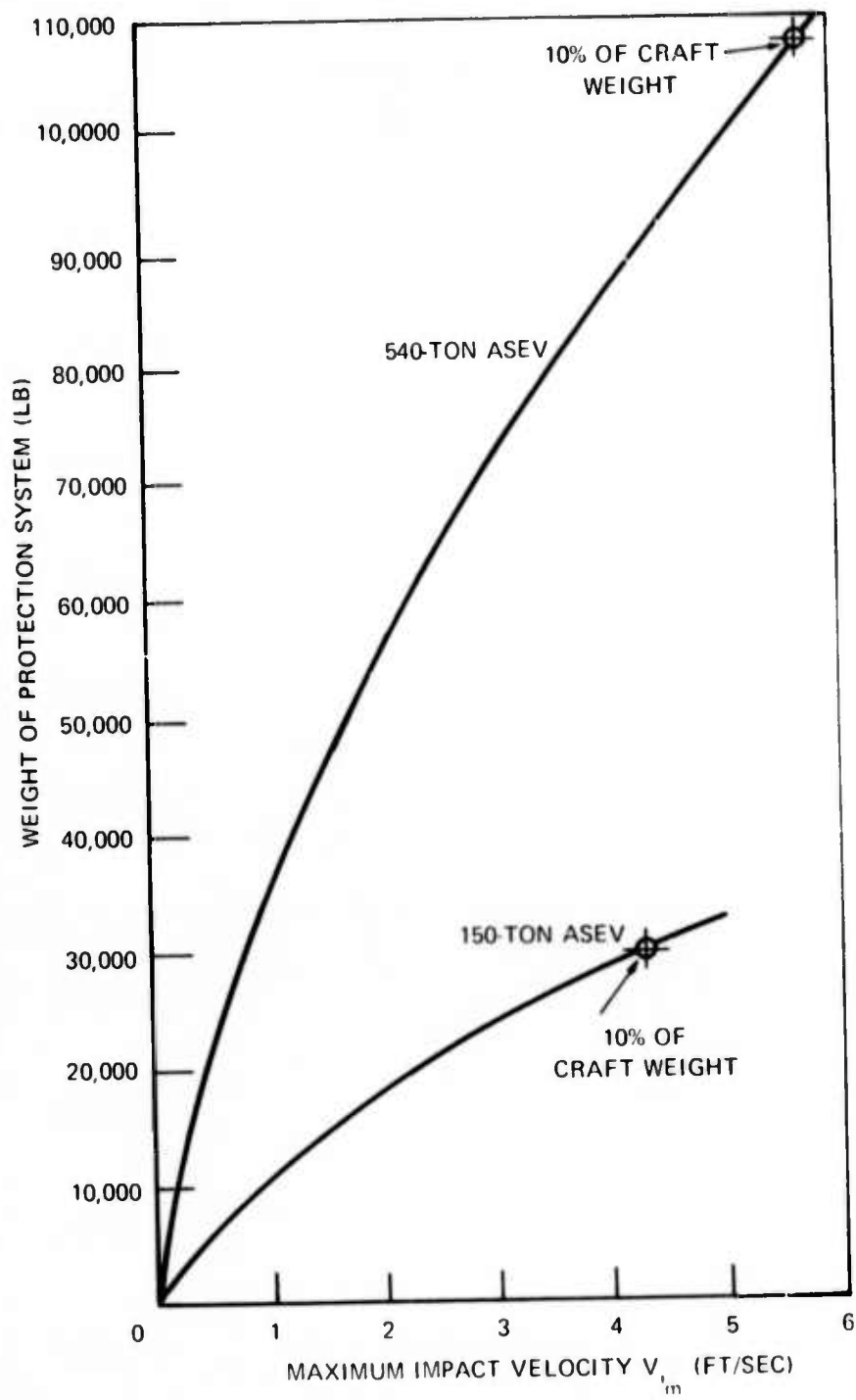


Figure 36 - Weight of Collision Protection System as a Function of Maximum Impact Velocity

Utilizing the suggested factor of safety and restricting the underbottom plating weight to 10 percent of the craft weight limit the allowable impact velocity to 3.45 and 4.65 ft/sec for the 150- and 540-ton craft, respectively (Figure 37).

## CONCLUSIONS

1. The energy absorption to rupture is a function of panel geometry.
2. Welding creates "weak links" where failure initiates.
3. Unstiffened (0.063-in. plate thickness) panels absorbed 1.21 and 0.70 times the respective energy absorption at rupture of (1 X 1) 1.5- and 3.0-in. web-stiffened panels of the same plate thickness.
4. Unstiffened (0.125-in. plate thickness) panels absorbed an average of 1.29 times the energy absorption at rupture of (1 X 1) web-stiffened panels (0.125-in. plate thickness) and 1.33 times the energy absorption of (3 X 3) web-stiffened panels of the same plate thickness.
5. The addition of flanges to web-stiffened panels generally increases the energy-absorbing capability significantly.
6. On the average, the addition of a layer of 2-lb/ft<sup>3</sup> urethane foam to a panel increases the energy-absorbing capability approximately 102 and 84 percent for stiffened and unstiffened panels, respectively. This increase is apparently the result of a distribution of the impact loading by the foam. However, the specific energy absorption for stiffened and unstiffened panels with a foam layer is comparable to that for the same panel without the foam layer because of the additional weight of the foam.
7. A 5086-H132 aluminum (1 X 1) panel with flanged stiffeners, plate thickness of 0.125 in., web height of 3.0 in., web thickness of 0.125 in., flange width of 2.0 in., and flange thickness of 0.125 in. displayed the highest material specific energy of all the (1 X 1) panels tested.
8. The (3 X 0) flanged-stiffened panel absorbed about 116 percent more energy for the same weight of panel. This panel was not selected for ASEV underbody definition since only one test was conducted for this geometry. Since the geometry does show promise, however, it is recommended that further work be done in the area of panels stiffened in this manner.
9. Provided deflection at rupture is known, theoretical load-deflection relationships for unstiffened and web-stiffened panels under static loading conditions show good agreement with experimental results.
10. There was good correlation between theoretical and experimental energy-absorbing capability based on average experimental deflection values at rupture.

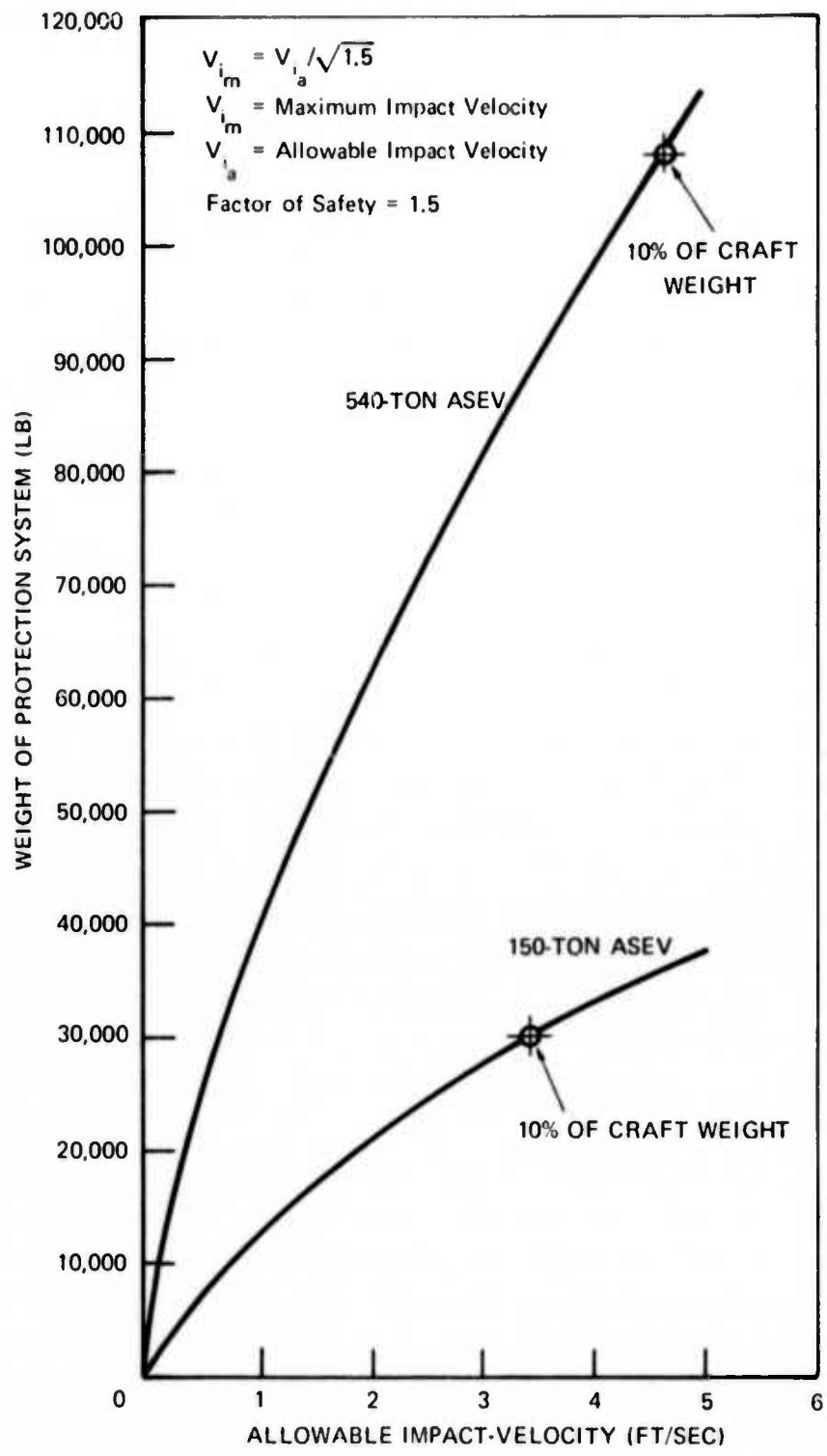


Figure 37 – Weight of Collision Protection System as a Function of Allowable Impact Velocity

11. A completely theoretical prediction of energy-absorbing capability for a given panel cannot be made at this time since it is not possible to accurately predict deflection at rupture. Further work in this area is needed.

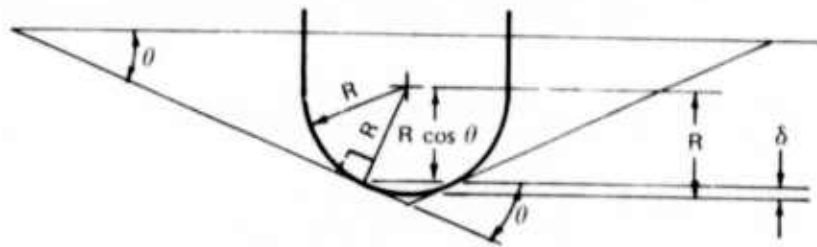
12. If the underbody weight is limited to 10 percent of the craft weight, allowable impact velocities of 3.45 and 4.65 ft/sec are reasonable to expect for 150- and 540-ton ASEV's, respectively.

13. To avoid longitudinal impact of the craft underbody and achieve absorption of the much greater energies associated with forward velocities, the dent sizes of the panels must be kept small. Dents in the tested panels at the point of rupture were generally 2.0 to 3.0 in. deep. These resulted in a dent wall at an angle of about 10 to 15 deg. This may be somewhat high to avoid longitudinal impact with the dent wall. Future work on oblique impact is needed to determine acceptable dent sizes.

#### **ACKNOWLEDGMENT**

The authors gratefully acknowledge the invaluable aid of Dr. M. Critchfield in the derivation of portions of the theoretical load-deflection definition.

**APPENDIX A**  
**DERIVATION OF PROTRUSION DEFLECTION DEFINITION**



The contact point is defined as that point where the panel is tangent to the impact obstacle surface.

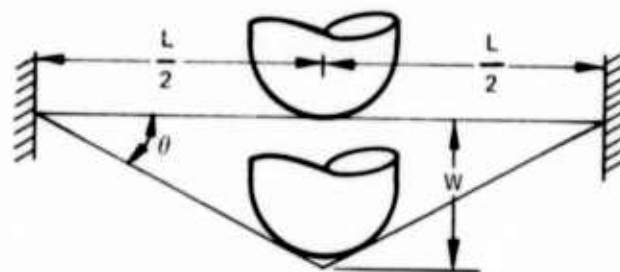
If the obstacle surface is a hemisphere of radius  $R$ , simple geometry relates the protrusion deflection  $\delta$  to the angle  $\theta$  and the radius of curvature of the obstacle  $R$ :

$$\delta = R - R \cos \theta \quad (\text{A.1})$$

Note that  $\theta$  is also seen to be the angle made by the straight-line approximation to the deflected shape of the panel which is approximated as:

$$\theta = \tan^{-1} \left( \frac{W}{L/2} \right) \quad (\text{A.2})$$

Here  $W$  is the total deflection of the center of the panel and  $L$  is the panel size, assuming that the protrusion deflection is small relative to  $W$ .



Combining Equations (A.1) and (A.2) yields the definition of the protrusion deflection:

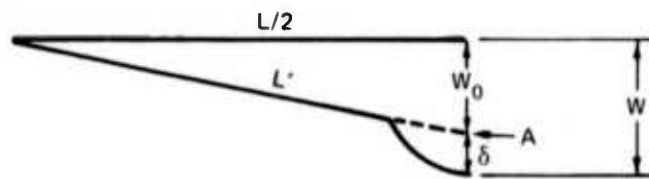
$$\delta = R [1 - \cos (\tan^{-1} (2W/L))]$$

**Preceding page blank**

**APPENDIX B**  
**DERIVATION OF MEMBRANE STRESS**

An expression is derived below for the membrane stress which results when a hemispherical head impacts a rectangular plate. The expression is most accurate for the case of a rectangular plate of high aspect ratio where the representation of the plate behavior by that of a plate strip is most valid. For the case of a square plate under consideration here, the plate strip model is more approximate.

The sketch shows the deflection profile for a plate strip taken through the center of the square plate and parallel to either of its sides. Because of symmetry, it is necessary to consider only one-half of the deflection profile as shown.



The deflection profile presented above contains a straight-line portion representing membrane behavior and a curved portion (local protrusion) which results when the plate conforms to the impacting head. Since the local protrusion  $\delta$  is a small part of the overall deflection  $W$  and is localized in nature, this protrusion is neglected in the deflection profile ( $W_0$ ) adopted for analytical purposes. This is accomplished by extending the straight-line membrane response region to point  $A$ . The strain associated with the elongation of the plate strip from its length  $L/2$  to its final length  $L'$  is given by

$$\epsilon = \frac{L' - L/2}{L/2} \quad (\text{B.1})$$

Now

$$L' = \sqrt{(L/2)^2 + W_0^2} = L/2 \sqrt{\left(\frac{2W_0}{L}\right)^2 + 1} \quad (\text{B.2})$$

Expanding Equation (B.2) in a binomial series, we obtain

$$\begin{aligned} \sqrt{\left(\frac{2W_0}{L}\right)^2 + 1} &= 1 + \frac{1}{2} \left(\frac{2W_0}{L}\right)^2 - \frac{1}{4} \left(\frac{2W_0}{L}\right)^4 + \dots \\ &= 1 + \frac{1}{2} \left(\frac{2W_0}{L}\right)^2 \end{aligned} \quad (\text{B.3})$$

since the term  $\frac{1}{4} \left(\frac{2W_0}{L}\right)^4$  and later terms may be neglected for small  $\frac{2W_0}{L}$ . Substituting Equation (B.3) into (B.2):

$$L' = L/2 \left\{ 1 + \frac{1}{2} \left(\frac{2W_0}{L}\right)^2 \right\} \quad (\text{B.4})$$

Then, insertion of Equation (B.4) into (B.1) yields

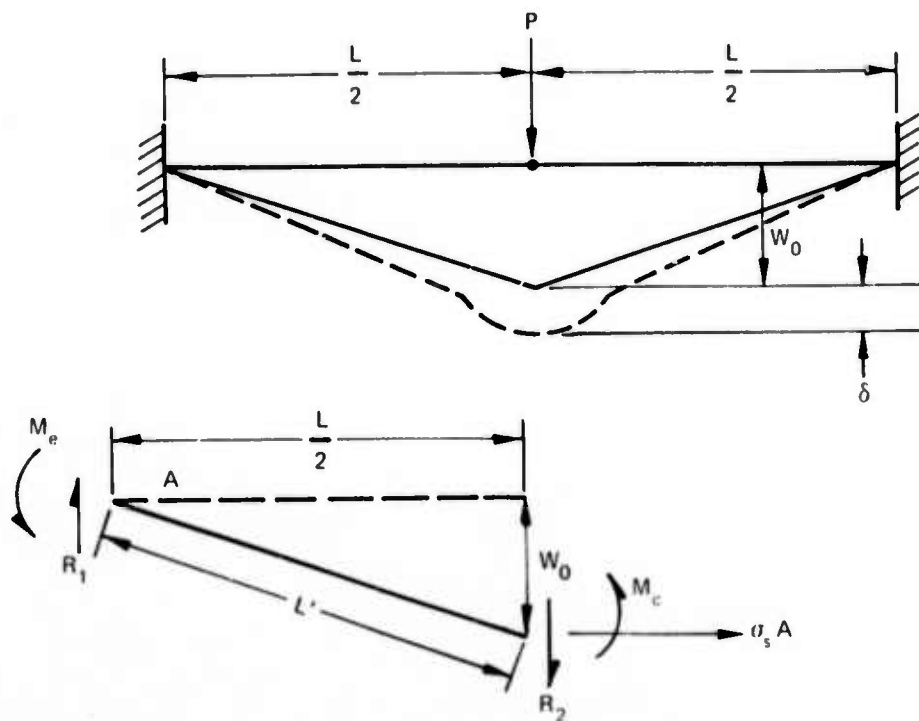
$$\epsilon = \frac{1}{2} \left(\frac{2W_0}{L}\right)^2 \quad (\text{B.5})$$

Therefore, since membrane stress and strain are related by Young's modulus  $E$  and since  $W_0 = W - \delta$ , we have

$$\sigma_s = E \left(\frac{W}{L}\right)^2 \left[ 2 - \frac{4\delta}{W} + \frac{2\delta^2}{W^2} \right] \quad (\text{B.6})$$

which is the final expression for membrane stress.

**APPENDIX C**  
**FREE-BODY DIAGRAM AND DERIVATION OF LOAD-DEFLECTION EQUATION**



$$\underline{\Sigma M_A = 0:}$$

$$M_c + M_c + \sigma_s A W_0 - \frac{R_2 L}{2} = 0$$

$$R_2 = [M_c + M_c + \sigma_s A W_0] \frac{2}{L} = 0$$

$$P = M R_2; P = 2 N R_2$$

$$P = \frac{4N}{L} (M_c + M_e) + \frac{4N}{L} (\sigma_s A W_0)$$

Here \$M\$ is the number of times the free-body segment is repeated in the structure and \$N\$ is the number of stiffeners passing through the collision point and \$N\$ equal to \$M/2\$.

**APPENDIX D**  
**DIMENSIONAL ANALYSIS OF ENERGY SCALING LAWS**

In order to extend the experimental results of the stiffened and unstiffened panels to different scale panels of the same geometry and material, scaling laws for the underbody collision phenomenon are derived by the dimensional analysis technique.

The first step in the dimensional analysis is to list all the variables relevant to the physical phenomena:

- $E_y$  = modulus of elasticity
- $G$  = shear modulus
- $\sigma$  = stress
- $L$  = characteristic length
- $V$  = impact velocity
- $M$  = mass
- $\rho$  = mass density of the material
- $E$  = energy
- $I$  = moment of inertia
- $A$  = acceleration
- $F$  = force
- $W$  = deflection

$$E = f(E_y, G, \sigma, L, V, M, \rho, E, I, A, F, W) \quad (D.1)$$

The dimensions of the variables are described in terms of the basic units of force  $F$ , time  $T$ , and length  $L$ .

<u>Variable</u>	<u>Dimensions</u>	<u>Coefficient</u>
$E_y$	$FL^{-2}$	a
$G$	$FL^{-2}$	b
$\sigma$	$FL^{-2}$	c
$L$	$L$	d
$V$	$LT^{-1}$	e
$M$	$FT^2 L^{-1}$	f
$\rho$	$FT^2 L^{-4}$	g
$E$	$FL$	h
$I$	$L^4$	i
$A$	$LT^{-2}$	j
$F$	$F$	k
$W$	$L$	l

The general equation for the dimensionless terms is written as follows:

$$(E_y^a, G^b, \sigma^c, L^d, V^e, M^f, \rho^g, E^h, I^i, A^j, F^k, W^\ell) = 0 \quad (D.2)$$

Equation (D.2) may be written in terms of the basic dimensions as follows:

$$[(FL^{-2})^a, (FL^{-2})^b, (FL^{-2})^c, (L)^d, (LT^{-1})^e, (FT^2 L^{-1})^f, (FT^2 L^{-4})^g, (FL)^h, (L^4)^i, (LT^{-2})^j, (F)^k, (L)^\ell] = 0 \quad (D.3)$$

Equation (D.3) may be rewritten as:

$$(F^{a+b+c+f+g+h+k}) (L^{-2a-2b-2c+d+e-f-4g+h+4i+j+\ell}) (T^{-e+2f+2g-2j}) = 0 \quad (D.4)$$

Since the exponents of the basic dimensions must be zero in any dimensionless term, the following equations may be written from Equation (D.4):

$$\begin{aligned} a + b + c + f + g + h + k &= 0 \\ -2a - 2b - 2c + d + e - f - 4g + h + 4i + j + \ell &= 0 \\ -e + 2f + 2g - 2j &= 0 \end{aligned} \quad (D.5)$$

Since there are three equations and twelve unknowns, nine of the unknowns are assigned arbitrary values and the remaining three are solved in terms of the other nine. When Equation (D.2) is rewritten with the new coefficients and grouped according to common coefficients, dimensionless terms result. These terms are the Buckingham Pi parameters and are the terms which must not change from model to prototype.

The dimensionless constants are as follows:

$$\begin{aligned}
\pi_1 &= E_y/\sigma \\
\pi_2 &= G/\sigma \\
\pi_3 &= M V^2/L^3 \sigma \\
\pi_4 &= \rho V^2/\sigma \\
\pi_5 &= E/\sigma L^3 \\
\pi_6 &= 1/L^4 \\
\pi_7 &= A L/V^2 \\
\pi_8 &= F/\sigma L^2 \\
\pi_9 &= W/L
\end{aligned}
\tag{D.6}$$

Since a geometric model is characterized by a scaled characteristic dimension, the model length is related to the prototype length by the following equation:

$$L_p = \lambda L_m \tag{D.7}$$

Since the model material is identical to the prototype material,  $\pi_5$  states that the energy-absorbing capability scales as follows:

$$\boxed{\lambda = \frac{E_p}{E_m}^{1/3}} \tag{D.8}$$

The other dimensionless constants define the scaling laws for other terms as follows:

$$\begin{aligned}
M_p &= \lambda^3 M_m \\
I_p &= \lambda^4 I_m \\
F_p &= \lambda^2 F_m \\
A_p &= 1/\lambda A_m \\
W_p &= \lambda W_m
\end{aligned}
\tag{D.9}$$

If the same material is used in the model as the prototype and the model is a geometric scale of the prototype, then the model response may be scaled up to describe the prototype response under the following conditions:

1. The effects of gravity are not important to the energy-absorbing process (since accelerations scale inversely as the scale factor).
2. Strain rate effects are not important since they cannot be properly scaled.
3. Residual stresses are not important.
4. Geometric details are accurately reproduced. Since the geometric details also scale by the scale factor, such surface irregularities in the model as finish, weld sizes and shapes, material flaws, and initial distortions are also scaled and may limit the degree to which the model results may be scaled.